

Investigation of Proximal Femoral Loads under Low Energy Impact Falls using Human Body Models

Ö. Cebeci, S. Checa

Abstract Low energy impact (LEI)-induced hip fractures are a growing problem, associated with high morbidity and mortality rates. Accurate modelling of such fractures could assist in developing preventive measures and mitigating incidences. Human body models open up new possibilities for computer modelling of such scenarios, allowing whole-body fall and impact simulations. The main objective of this study was to evaluate the LEI performance of THUMS V502 and to investigate the impact-induced proximal femur loads. Initially, the model performance was tested and verified for the primary musculoskeletal performance, fall kinematics and impact behaviour. Using the verified model, various fall configurations, reported in observational studies, were simulated applying different muscle contractions patterns. Subsequently, simulation results were analysed regarding the whole-body kinematics, proximal femur loads, and the influence of muscle activations. Overall, simulations showed comparable results with the available literature. In summary, THUMS V502 enables a detailed investigation of LEI fall-induced femoral loads, including realistic fall kinematics, impact behaviour and muscle activations.

Keywords Active Muscles, Fall Kinematics, Human Body Modelling, Low Energy Impact Falls, Proximal Femur Loads.

I. INTRODUCTION

Low energy impact (LEI)-induced hip fractures pose a major threat for elderly people worldwide [1]. Such fractures are associated with high morbidity and mortality rates [2], and also place serious strain on the healthcare system. For these reasons, it is necessary to understand LEI-induced hip fractures in order to detect high-risk patient groups and develop strategies that can mitigate fracture rates. Current clinical risk assessment tools focus mainly on bone quality measurements and some basic anthropometric parameters [3-4]. The accuracy of those methods is limited [5]; however, due to the complexity of LEI-induced hip fractures, which include several sequential events and cover different space-time scales. In addition, the subject-specific and stochastic nature of fall events poses further challenges for reliable fracture assessments.

Hip fractures occur when the applied load exceeds the femur strength. Accordingly, there exists a long tradition of research on both fall-induced femoral loads and femur strength. Concerning the fall-induced femoral forces, the literature can be categorised into voluntary experiments, ex-vivo studies, observational studies, and computer modelling approaches. The voluntary fall experiments are mostly carried out with healthy young adults falling from low or standing height and using a thick protective pad. Despite their limitations, these experiments provide valuable information for model validations [6-7]. Concerning the higher force levels, the ex-vivo experiments are the only option considering the obvious ethical restrictions of the voluntary studies. However, due to the missing in vivo conditions, such as muscle activations and skeletal stability, rigid boundary conditions are often applied for the sake of reproducibility. Reducing a fall event to a free-falling mass or an inverted pendulum are some of the common strategies applied in the ex-vivo studies [8-9].

Despite being a recently introduced field, the observational studies have improved our understanding of the fall kinematics and patterns, closing the gap between the voluntary falls and the actual reality of the real-world elderly falls [10-11]. The published results have shown that the majority of the falls take place as a result of incorrect weight shifting, and the average impact velocity tends to be lower than the observed velocities in the voluntary falls [12].

The available modelling approaches largely deal with the fall kinematics and the impact separately. Abstractions and rigid boundary conditions similar to those used in experimental studies are often applied. Briefly,

the fall kinematics are represented in most of the studies using rigid multibody systems or based on the reverse pendulum falls [7]. Besides these, some studies try to predict fall kinematics using proportional–integral–derivative (PID) controlled kinematic chains [13]. The most common approach to predict the impact forces, which can be later applied to finite element (FE) models for more advanced fracture assessments, is to use analytical impact models [5]. Apart from these, some recent studies have represented the fall kinematics and the impact using explicit FE models to predict the impact forces and the femur fractures more accurately [8].

Although valuable progress has been made in terms of the impact force and the fracture predictions, inaccurate consideration of the joint reactions, pre-impact movements, preventive reactions, active muscle loads, fall- and subject-specific aspects remain as the main limitations of the available modelling approaches.

The main objective of this study is to investigate the proximal femur loads induced during LEI falls using human body models (HBMs). The available HBMs are developed for occupant safety applications and validated for high energy impact load cases [14]. To the authors' knowledge, HBMs have so far only been used in a few unpublished studies to investigate the fall-induced hip impact forces. In general, HBMs enable a comprehensive investigation of the impact situations, eliminating some of the above-mentioned limitations.

In this study, modelling abstractions like isolated femur-hip complex or restricted fall kinematics, as well as the rigid boundary conditions, are avoided. Besides that, the whole-body fall kinematics and the influence of the muscle contractions are regarded as well. Through this study, the following research questions are addressed.

- To what extent can HBMs be used to investigate LEI falls?
- How do variations in fall configuration and boundary conditions influence proximal femur loads under LEI falls?
- How do different muscle activation patterns influence proximal femur loads and hip joint stability under LEI falls?

II. METHODS

In this study, due to its detailed muscle modelling and the reported validation cases, THUMS V502 was used [14]. All simulations were carried out using LS-Dyna version 931 in double precision [15]. Concerning the bone material modelling, the default `"*MAT_PIECEWISE_LINEAR_PLASTICITY"` definition was used and, for simplicity, bone failure was not included. The used material model allows rate-dependent elastoplastic deformations based on the defined elastic parameters, yield stress, strain rate parameters and effective plastic strain-stress values. Since the original THUMS V502 had been mostly validated for high energy trauma cases [14], the model performance was further verified for postural stability and LEI behaviour. Using the verified model, various fall configurations, reported in the observational studies, were simulated, applying different muscle contractions patterns as mentioned next. In all simulations, constant gravity is applied, and the floor is model as a rigid plane. A coulomb friction constant of 0.6 is used for all external contacts, considering a high friction floor treatment as often observed in hospital or care facilities [16-17]. The simulation results were analysed in terms of the kinematics and the proximal femur loads. Finally, the results were compared with the available literature.

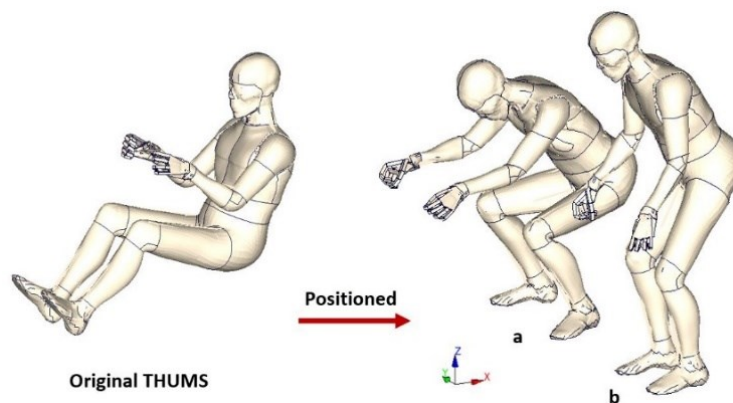


Fig. 1.: Original THUMS model and positioned models, i.e. a) Squatting b) Flexed standing

Model positioning

All models presented in this work were positioned using the IAT PROMSIG [18] tool. To briefly mention, the positioning process consists of 2 main steps. First, the desired target position was defined in a pre-processing software (PRIMER; Oasys Ltd.) with the help of a kinematic chain provided by PROMSIG. Later, a positioning model, which is modified to ensure physiologically plausible deformations, was moved into the target position with prescribed motions (*BOUNDARY_PRESCRIBED_MOTION) starting from the original position (Fig. 1). In the end, nodal coordinates of the original HBM were adjusted based on the last frame of positioning simulation.

Musculoskeletal model testing

It is almost intuitive that without the muscle activations (MAs), a fall from standing height looks rather like a straight vertical fall. Therefore, the primary musculoskeletal model behaviour was tested using the default and adjusted muscle controller parameters in the forward flexed standing and squat postures (Fig. 1 a-b) to ensure postural stability under constant gravity. Muscles defined in THUMS V502 are modelled with truss elements and a Hill-Type material model (*MAT_MUSCLE) which accounts the contractile, passive and damping stress components. Muscles can be modelled with or without MAs by accounting or eliminating the contractile stress components, respectively. MAs can be included either using predefined activation levels or using the provided muscle controller. The dimensions of the muscle elements are defined based on the physiological cross-sectional area of the corresponding muscles.

The muscle controller implemented in THUMS V502 adjusts the MA levels to sustain a predefined posture. In detail, the body is considered as different segments such as head, thorax, pelvis, upper legs, lower legs, feet, upper arms, lower arms and hands (Fig. 2-a). The orientation of each segment is defined based on a local coordinate system, and the difference between these segmental orientations are considered as current joint angles (JAs) namely the neck, torso, hip, knee, ankle, shoulder, elbow and wrist angles. JAs are calculated based on the coordinate system closer to the pelvis, as demonstrated in Fig. 2-b. Based on the difference between current JAs and the defined target JAs, a PID controller generates control signals for joint rotations. Later these control signals transform into corresponding MAs using a muscle coordination matrix and sigmoid functions. Muscle coordination matrix defines the percentual contributions of each muscle for distinct joint rotations, and sigmoid function ensures that the MA signal changes between 0.01 and 0.99 (Fig.2 c-d). The controller character can be adjusted varying the PID gains.

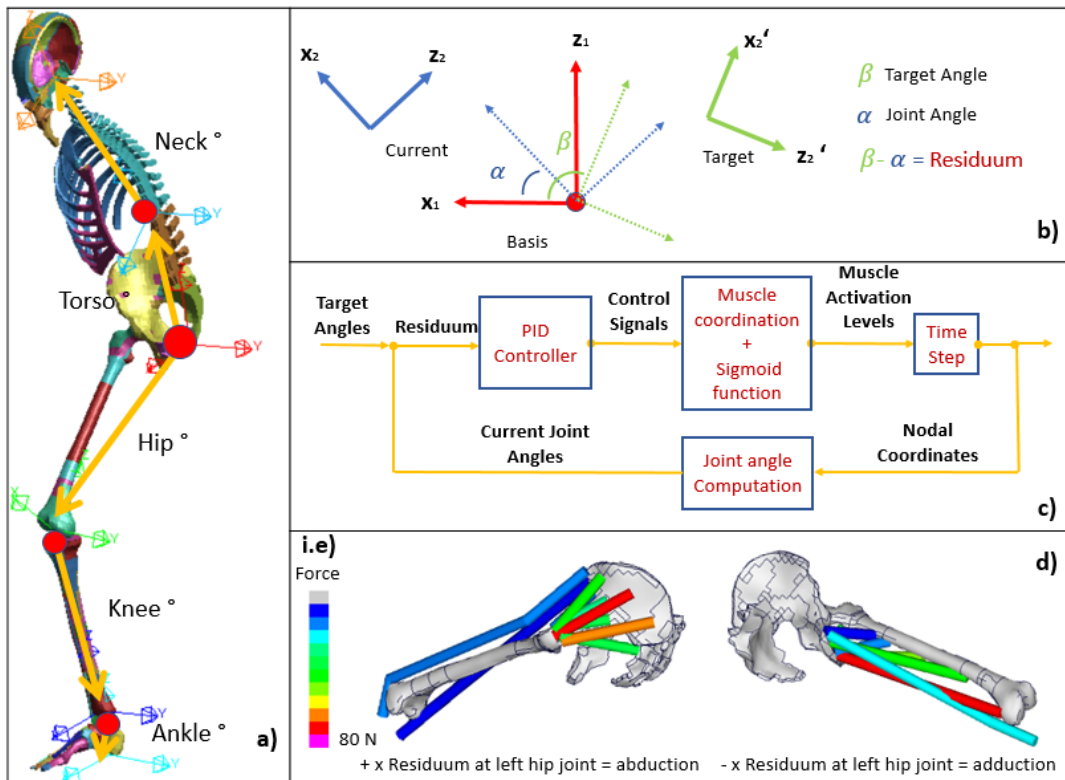


Fig. 2. a) Body segments and the coordinate systems, b) Current and target joint angles, c) PID control scheme, d) Muscle coordination

Default muscle control strategy is designed to sustain model position in seated postures under low g loading. For this reason, as default, target JAs (defined by the user in input deck) describe the initial posture (the positioned model), and corresponding MAs are first initiated following the postural change (target JA \neq current JA). This strategy was not able to sustain the standing postures under constant gravity since it provides no initial MAs, which is essential in standing postures.

In order to overcome this problem, posture-specific target JA offsets were tested. For example, having an initial hip JA of -20° in the y-axis and defining a target JA of 10° for the same rotation component, which we call 30° target joint angle offset (TJAO) as often mentioned in the following sections, would activate the hip extension muscles. Using this principle, initial MA levels can be defined based on the TJAOs. Besides that, the PID gains can be adjusted to influence the control and, therefore, MA characteristics for the desired musculoskeletal performance.

Forward flexed standing and squatting models were positioned as described previously. TJAOs were defined for neck, torso, hip, knee and ankle joints (Fig. 2-a). Table I and Table II show the tested TJAOs and the PID parameters. The PID gains for neck and torso were increased to enable stronger upper body MAs. For the upper extremities, the default parameters were used. Given TJAOs and PID parameters were determined by manual calibration.

TABLE I TARGET JOINT ANGLE OFFSETS (TJAOs)			TABLE II PID PARAMETERS	
Joint	Squat	Forw. Flexed Stan.	Parameter	Value
Neck	20° Extension	10° Extension	NECK_K_P,I,D	10.0,10.0,10.0
Torso	45° Extension	20° Extension	TORSO_K_P,I,D	10.0,10.0,10.0
Hip	75° Extension	30° Extension	KNEE_R,L_P,I,D	1.0, 0.0, 0.0
Knee	90° Extension	30° Extension	HIP_R,L_P,I,D	1.0, 0.0, 0.0
Ankle	20° Extension	30° Extension	ANKLE_R,L_P,I,D	1.0, 0.0, 0.0

The reference joint reaction force results, used in model evaluations, were provided from the ORTHOLOAD database [19] using the trial number H2R_060711_1120 and H3L_260811_1_131 for squat and flexed standing cases, respectively. The first trial enabled a good comparison with the simulated squat case since a similar posture was statically sustained. In the second trial, the test subject does not sustain the forward flexed posture statically; however, changes his posture between straight standing and squatting. It can be expected that during forward flexed standing, due to the MAs, higher joint reaction forces than straight standing occurs. Similarly, during the rising phase of squatting, higher joint reaction forces than the forward flexed standing should be observed. The loading range to evaluate forward flexed standing was defined using this principal based on the force results at 4.9s and 6.32s. In both simulations, the joint reaction forces were measured in the same local coordinate system as it was measured in the trials.

The tested flexed standing and squatting postures are described in terms of the nodal coordinates in Appendix A for completeness.

Low energy impact verifications

Two different verifications for LEI falls were performed.

(1) Low height voluntary falls: the impact behaviour was initially tested based on the reported low height voluntary falls by Lou *et al.* [7]. To describe briefly; in the experiments, voluntary subjects were brought into predefined fall postures, which ensures an initial ground contact over the trochanter, using a full-body harness and adjustment strings. An electromagnetic release enabled the fall initiation. Initial fall posture and the fall kinematics were measured with a motion capture system and reflective markers. Subject anthropometry was measured using dual-energy X-ray absorptiometry (DXA) images.

Regarding the matching anthropometric measures, we used the "Subject 1" as a reference. A comparison between "Subject 1" and THUMS V502 is given in Table III. Authors presented ground reaction forces for "Subject 1" from 50mm fall height without protective padding. The simulation model was positioned (see model positioning) according to the published supplementary material [20], and the measured ground reaction forces were compared with the experimental results.

Initially, the positioned simulation model had a higher initial fall height due to the anthropometric deviations. In order to ensure the same fall height and the impact velocity, a massless height adjustment element between

the force transducer and the trochanteric soft tissue (TST) is integrated in the simulation model as shown in Fig. 3. More detailed information regarding the positioning provided in Appendix B1.

(2) Ex-vivo falls: further verification of the model was conducted based on the ex-vivo study reported by Fleps *et al.* [8][21]. The presented experimental setup enables reproducible ex-vivo fall tests from standing height using a state-of-the-art reverse pendulum structure. In the experiment, femur-pelvis complex specimens were gathered from post-mortem human subject. Pelvic soft tissues were replaced by a surrogate gel and inertia elements (distributed mass). Prepared specimens were fixed with a fall-guiding structure. In terms of the fall boundary conditions, a guiding structure constrained the relative motion of both lower limbs (including the inferior femur) and the pelvic motion in the sagittal plane. Right before the impact, all constraints (out to the spherical joint on the impact side foot) were eliminated to realise a constraint-free impact. The impact velocity of 3.1 m/s (± 0.1 m/s) was ensured by adjusting the initial fall heights of the specimens.

Due to the anthropometric similarities, the results of "specimen H1402" were utilised in our study. A comparison between the THUMS V502 and the specimen H1042 is given in Table III. Once again, the simulation model was positioned as described in the corresponding publication [21]. Similar boundary conditions for the fall and impact phase were defined, as demonstrated in Fig. 4-a and 4-b, to realise the same controlled fall kinematics. Impact simulation was restarted following the fall phase using the updated boundary conditions. Initial velocities of the impact model were adjusted to ensure the identical impact velocity of 3.1 m/s.

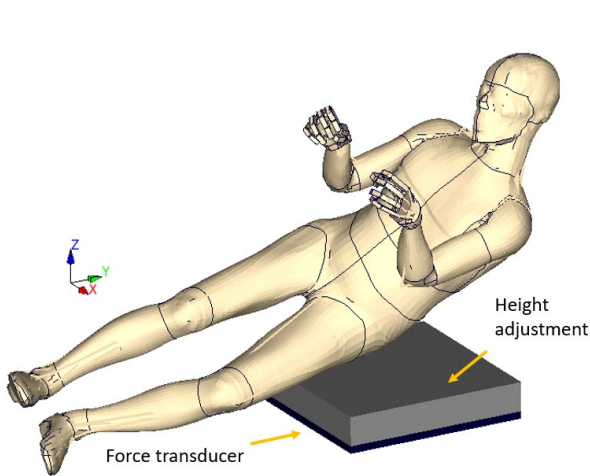


Fig. 3. Voluntary fall simulation from 50mm fall height based on Lou *et al.* [7]

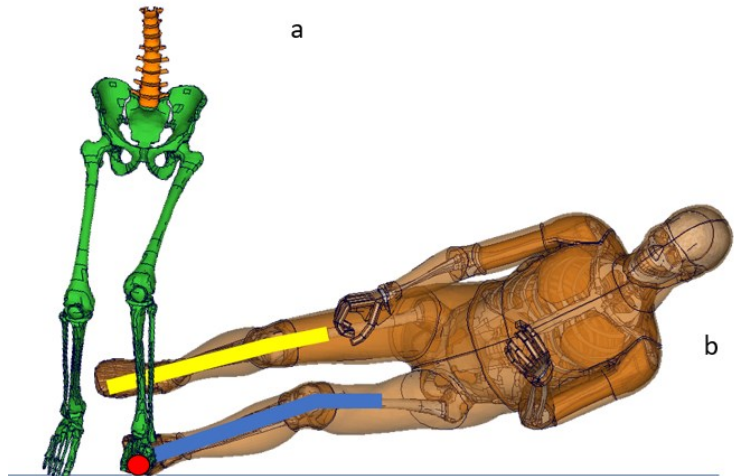


Fig. 4. Ex-vivo fall simulation from standing height based on Fleps *et al.* [8][21]. a) Fall phase: Green parts were constraint against the relative motion. Orange parts were constrained in the sagittal plane. b) Impact Phase: Yellow and blue lines show the rigid lower limbs.

TABLE III

ANTHROPOMETRIC COMPARISONS

	Age	Height (m)	Weight (kg)	Shank (m)	Thigh (m)	Trunk (m)	TST Thick. (mm)
Subject 1	Young Adult	1.73	77.0	0.43	0.44	0.84	18.0 (defined)
H1402	70	1.75	68.0	-	-	-	14.0
THUMS	-	1.75	77.0	0.55	0.43	0.79	30.0 (original)

Authors provided ground reaction forces for the ex-vivo fall experiments and validated specimen specific FE models with linear and non-linear bone properties. Both the experimental results and the simulation models yield no visible fracture for the specimen H1402. The reported FE model with non-linear bone properties showed a similar peak force (+5% error) with the experimental results (CORA score: 0.595). However, the experimental results showed a sharp peak force drop, suggesting that, although not visible, there might be fracture relevant deformations.

Since our model includes the whole body, it is difficult to provide a comparison using the ground reactions. Therefore, the results were evaluated in terms of the FN forces. Also, considering that the main focus of this study is proximal femur loads, FN forces provided more applicable results. In another publication [22], based on a similar ex-vivo experiment (different specimens) and simulations, authors had been demonstrated that the ground

reaction and FN forces follow a similar trend. Regarding this, since FN force curves had not been provided for the specimen H1402 (both for experiment and simulations), the result used for comparison was derived by scaling the provided ground reaction curves based on the reported peak FN force value of the FE model.

Considering that in our study an elastoplastic bone modelling without fracture is used, we utilised the provided FE results with non-linear bone properties (rather than linear model), which yields no fracture for H1402, as a reference to enable a more relevant comparison.

The reported ground reaction (experimental and FE results) and the derived reference FN forces, as well as the detailed positioning information, are provided in Appendix B2.

Initial results showed that the default TST modelling should be adjusted for more realistic impact behaviour. Therefore, the TST thickness and the material model were modified to improve the impact behaviour. The TST thickness was adjusted based on the measurements presented by Levine [23] (this value is also later used in impact simulations) and the reported specimen thickness by Fleps [8] for the voluntary and ex-vivo fall simulations, respectively (TABLE III). Concerning the constitutive modelling of the TST, the Ogden rubber model, a commonly used material in soft tissue modelling [24], was implemented and calibrated for the above-mentioned experiments, while in the original model the so-called "Mat_Simplified_Rubber" [14] was used. The calibrated material definition and a literature comparison are provided in Appendix B3.

In order to avoid the negative element Jacobian problems and to increase the model robustness, default (type 0) tetrahedral elements with 5 mm average element size were used in TST modelling. Re-meshing was carried out in ANSA pre-processing software (Ansa 17.1.0; Beta CAE Systems). A mesh sensitivity test was conducted to prove that FN forces were not altered by the meshing strategy and the element formulation. Results of the mesh sensitivity test and a further discussion concerning the used element formulation is provided in Appendix B4. The modifications mentioned above were applied on whole pelvic soft tissues (a superset of TST) sustaining the mesh compatibility with the surrounding soft tissues. The TST thickness is adjusted by morphing the initial form, so that the pelvic soft tissue form remained unchanged in other regions.

All models described in this section were simulated without muscle activations.

Initial fall configuration and fall simulations

The observational studies have suggested that the majority of the falls occur from the standing height due to the incorrect weight shifting without balancing devices. Also, hand and knee contacts, as well as active squatting, were often observed and considered as protective actions [12][10]. Based on this evidence, various initial fall configurations (Table IV) from standing height were generated. In detail, initial positions consist of the forward, backward, and lateral fall initiations, including the different arm and knee postures to model reported protective actions.

All initial postures were generated starting from the, previously mentioned, forward flexed standing posture with a minimum joint angle (JA) deviation as possible. For completeness, those deviations are provided in Appendix A. As positioning criteria, in all fall configurations, the centre of gravity (CoG) projection on the floor stays outside of the base of support (2.5 ± 1.5 cm). Besides that, based on the initial fall posture, the initial anterior superior iliac spine height ranged between 83 and 93 mm. All initial fall configurations and their base of supports boundaries are presented in Fig 5.

In addition to these configurations, based on the first lateral fall case (lateral-a, see TABLE IV), a stumbling scenario was simulated with an anterior initial velocity of 0.5 m/s and two different 5 cm high obstacles on the floor. A more detailed description of the boundary conditions for this case is provided in Appendix D3.

TABLE IV
FALL CONFIGURATIONS

Forward	Lateral	Backward
<i>a) Protective arms</i>	<i>a) None /+ Stumbling</i>	<i>a) None</i>
<i>b) Protective arms + flexed knee</i>	<i>b) Protective arm</i>	<i>b) Protective arms</i>
	<i>c) Flexed knee</i>	<i>c) Active Squatting</i>
	<i>d) Protective arm + flexed knee</i>	<i>d) Protective arms + Active Squatting</i>

The previously presented muscle controller setup, namely the target joint angle offsets (TJAOs) and the PID gains, utilised for the forward flexed standing was used in all fall configurations as the basis. Only the Torso TJAO was reduced 10° to decrease upper body muscle activations for more realistic fall kinematics (otherwise models

brace unrealistically during the fall). As a protective action, neck and torso TJOs were defined in fall opposite directions. This strategy bended the upper body and neck slightly on the fall opposite direction. For simplicity, the target joint angles kept constant during the falls. Apart from the basis PID gains (PID Set 1), a second PID parameter set (PID set 2) was defined (determined by manual calibration) with reduced progressive gain values for the lower limbs, to model decreased the muscle activations. All TJOs and the PID parameters used in fall simulations are provided in TABLE V. For the upper extremities; the default parameters were used.

Apart from those, in order to reduce the computation time in the fall simulations, bone structures, excluding cartilages, were converted to rigid bodies, which increased the critical time step.

TABLE V
TARGET JOINT ANGLES OFFSETS AND ADJUSTED PID GAINS USED IN FALL SIMULATIONS

Target Joint Angle Offsets		Adjusted PID Parameters		
Joint	Offset	Parameter	PID Set 1	PID Set 2
Neck	10° Extension / Flexion / Lateral Bend	NECK_K_P,I,D	10.0, 10.0, 10.0	10.0, 10.0, 10.0
Torso	10° Extension / Flexion / Lateral Bend	TORSO_K_P,I,D	10.0, 10.0, 10.0	10.0, 10.0, 10.0
Hip	30° Extension.	KNEE_R,L_P,I,D	1.0, 0.0, 0.0	0.6, 0.0, 0.0
Knee	30° Extension.	HIP_R,L_P,I,D	1.0, 0.0, 0.0	0.6, 0.0, 0.0
Ankle	30° Extension.	ANKLE_R,L_P,I,D	1.0, 0.0, 0.0	1.0, 0.0, 0.0
Upper Extremities	0°			

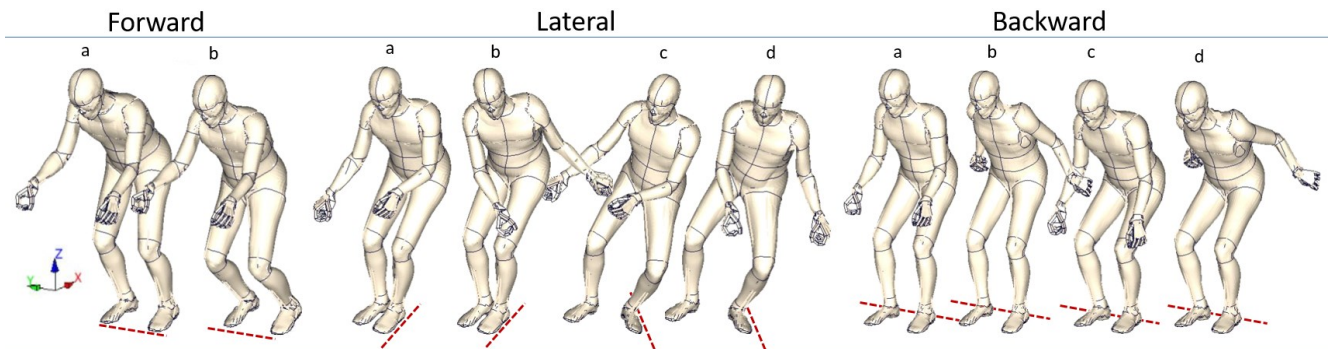


Fig. 5. Initial fall configurations and the base of support boundaries (red lines)

Impact simulations

One of the important advantages of simulating the fall and the impact with the same FE models is the excellent simulation restart possibilities. In this case, having the fall simulation results, the impact simulations could be restarted using the full deformable model, including the impact-specific adjustments (Ogden material, TST thickness of 18mm) described previously. In all fall configurations, the impact simulations were conducted based on this approach. The fall simulations were terminated shortly before (0-5ms) the initial hip, upper leg or knee contact and the impact simulations were restarted from this state on.

Since the fall simulations were conducted using rigid bones and increased critical time step to reduce the computation time, the modified TST modelling was only used in impact simulations due to its smaller element size. Following the fall simulations, TST is positioned and deformed into the new target position with the help of an intermediate simulation (using prescribed motions). Initial velocities for the modified TST was defined based on the average pelvic velocity neglecting the local velocity variations (no deformation or kinetic energy fluctuations were observed). Impact simulations were normally terminated 20 ms after the head impact. Based on the fall configurations, the fall and impact simulation normal termination time varied between 0.794 - 1.350 s and 0.08 - 0.3 s respectively.

Due to the current literature, there is no concrete evidence regarding the muscle activations at the instance of a fall induced impact. Considering this, the muscle activations were not used (passive muscle state) in initial impact simulations to avoid misleading effects. However, the influence of the hip muscle co-contractions was investigated later in lateral fall cases with high FN forces as described in the following section in detail.

Body postures at the instant of the impact were quantified based on the angles between segmental body planes and the fall floor (referenced as "segmental angles"). Definitions of the segmental body planes are provided in

Table VI and visualised in Appendix C. Additionally; results were evaluated in terms of the FN and L5 vertebral loads, as well as the pelvis and the head kinematics.

Impact simulations were generated among the fall configurations based on their relevance to the hip impact. Therefore the fall cases, which does not yield hip impact or which yield very similar fall kinematics with the other falls (in terms of the hip velocity and the segmental plane orientations) were not included. A detailed list concerning the data inclusion and model properties is provided in Appendix E.

TABLE VI
Segmental Planes

Segmental Planes	Definition	Purpose
<i>Femur Neck Plane</i>	<i>Femur Neck Axis + Anatomical Femur Axis</i>	<i>Defines the greater trochanter orientation</i>
<i>Sagittal Pelvic Plane</i>	<i>Sagittal Pelvic Plane</i>	<i>Defines the lateral pelvis orientation</i>
<i>Anterior Pelvic Plane</i>	<i>Left, Right ASIS, Pubic Symphysis</i>	<i>Defines the anterior-posterior pelvis orient.</i>
<i>Sagittal Torso Plane</i>	<i>Pubic Symphysis, Posterior T6, Sternum</i>	<i>Defines the lateral torso orientation</i>
<i>Posterior Torso Plane</i>	<i>Left-Right Super.-Post. Sacrum, Post.T6</i>	<i>Defines anterior-posterior torso orient.</i>

Influence of the muscles contractions during and after the initial impact

Hip muscles are not only responsible for motor functions, but they also stabilise the hip joint [25]. Moreover, it is suggested that muscle co-contractions can reduce FN moments [26]. In order to test this hypothesis, contraction of all hip muscles along with co-contraction of the flexion-extension, adduction-abduction and rotator muscle groups were compared with the passive muscular state, in lateral fall-induced impacts which yield fall induced FN forces above 3.5 kN. The list of the accounted fall configurations is given in Appendix E. Considering the poor neuromuscular state of the elderly, a basis activation level of 0.2 was applied for the corresponding motion groups (flexion-extension, adduction-abduction and internal-external rotation). The activation level of the individual muscles was defined based on the applied basis activation level (0.2) and muscle coordination matrix, as provided and explained in Appendix B5 in detail. In the end, results were evaluated in terms of the FN forces and moments. A 2-tail paired T-test was conducted where the FN loads without MAs were compared with the FN loads of each co-contraction pattern. Results showed the significance of the changing FN force and moment due to the muscle co-contractions. Significance level was set to $p=0.05$.

In the absence of MAs, almost all fall simulations, which terminated normally, revealed severe head impact due to the high head impact velocity. In detail, the measured mean head velocity and Head Injury Criteria (HIC) [27] (time range = 36ms) values were 7.13 m/s (4.34-11.16) and 2628 (460-9450), respectively. The published average head velocity in elderly falls was, however, far less than the simulation results (on average, 4.1 m/s) [10]. It can be suggested that this substantial difference cause by the missing MAs in impact simulations. In order to test this hypothesis and investigate the influence of the protective MAs with respect to the head kinematics, a protective flexion strategy was defined in a backward fall (backward-d, see TABLE IV) induced impact simulation. Protective flexions are applied using the previously presented muscle control strategy along with the PID parameter set 1 (PID Set 1 in TABLE V). The utilised TJAOs are given in Table VII.

TABLE VII
TJAOs for Protective Flexion

Joint	TJAO	Joint	TJAO
<i>Neck</i>	<i>20° Flexion.</i>	<i>Hip</i>	<i>20° Flexion</i>
<i>Torso</i>	<i>20° Flexion.</i>	<i>Rest of the joints</i>	<i>0°</i>

Load measurements, evaluation methods and data overview

Concerning the acceleration, velocity, force and moment outputs, a detailed description is provided in appendix C. To mention briefly; body loads were measured using DATABASE_CROSS_SECTION definitions and the kinematic entities captured from the CoG of the corresponding body part.

All curve comparisons provided in this work are quantified with CORA (Correlation and Analysis) scores using the CORAplus Software (pdb – Partnership for Dummy Technology and Biomechanics) based on the ISO 18571 norm [28]. CORA score describes the quality of matching for two non-ambiguous curves based on the phase, size

and the shape of the curves. CORA ratings of 1.0-0.86, 0.86-0.65, 0.65-0.44, 0.44-0.26, 0.26-0.0 are considered as excellent, good, fair, marginal, and unacceptable, respectively.

The box plots used in result evaluations are generated in Microsoft Excel 365 (Microsoft Corporation), which demonstrates the average, median, first and third quartiles (Q1, Q3), maximum and minimum values (Q1-1.5×IQT and Q3+1.5×IQT; IQT: interquartile range) as well as the outliers of the evaluated datasets.

An overview of all simulation models, including model properties and the data inclusion is given in Appendix E.

III. RESULTS

Musculoskeletal model testing outcomes

Muscle controller parameters provided in TABLE I and II showed sufficient postural stability in the flexed standing and squat postures. Both of the models sustained their position more than a second without any critical disturbance in their posture. Since the average fall duration had been reported as 1 s [12], this performance was considered to be acceptable. In the squat case, the quadriceps force and the gluteus maximus activation level, as well as the joint reactions forces, showed good agreement with the literature (Table VIII). Forward flexed standing joint reaction forces were, apart from the x force component, within the defined force ranges, suggesting that, beyond the postural stability, simulations also yield physiologically plausible MAs (Table VIII).

TABLE VIII

FLEXED STANDING LITERATURE COMPARISON

TABLE VIII

SQUATING LITERATURE COMPARISON

	Sim. Result	Literature (ranges)	Ref.		Sim. Result	Literature	Error	Ref.
				<i>Quadriceps force</i>	4.9 BW	4.94 BW	-0.8%	[29]
				<i>Gluteus Max. Act.</i>	0.81	0.71	+14%	[30]
<i>Joint reaction</i>	0.16/ 0.22/ 0.94	0.26-0.35/ 0.07-0.44/ 0.68-1.5	[19]	<i>Joint reaction</i>	0.0 / 0.4 / 1.7 (BW)	0.23 / 0.4 / 1.57 (BW)	+6% (residual)	[19]
(x/ y/ z)				(x/ y/ z)				

Impact model verification results

The simulation results of the modified models were compared with the corresponding literature in Fig. 6 and Fig. 7. In both trials, the calibrated Ogden model was used, and TST thickness was adjusted based on the literature as well as the reported specimen thicknesses. CORA scores provided in this section are given for 0-30ms time range to focus our evaluation to trochanteric impact.

Figure 6 shows the predicted ground reaction forces for low height voluntary fall with 18 mm TST thickness when using the THUMS default material model and the newly implemented Ogden model, as well as the original THUMS V502. The Ogden model showed a closer agreement with the experimental data (CORA Score 0-30ms: 0.842). The default model, on the other hand, yielded a fast peak and force drop following the impact due to the compressible material behaviour (CORA Score 0-30ms: 0.659).

In Fig. 7, the predicted femur neck force when using the Ogden model and the original material model of THUMS V502 is compared based on data derived from Fleps [8] as previously described in methods. The original data is provided and further discussed in Appendix B2. Predicted data yield +10% and 12% peak value error (CORA Score 0-30ms: 0.671 and 0.461) respectively for Ogden material and original THUMS material with 14mm TST. It can be suggested that this difference caused by the mass deviation (TABLE III) between THUMS and the original specimen (+13 %).

As a result of the higher impact force and the thin TST (14mm), the influence of the TST material was not as dominant in falls from standing height as it was in the low height fall simulations. However using the Ogden model in original THUMS V502 which have a TST thickness of 30 mm, results yield a peak FN force of 5.05 kN where the original THUMS V502 yields 5.94 kN (Fig. 7). Comparing these values with the 14mm TST results, a force drop of 77.5 N/mm and 26.9 N/mm for Ogden and original material model of the THUMS V502 can be calculated. Concerning the TST thickness influence on the FN forces, Robinovitch and colloquies [31] had been reported 71N/mm trochanteric force reduction due to the increase in tissue thickness. This value poses a better agreement with the implemented Ogden material model results (+9% error).

For completeness, a modified TST (as defined in methods) with 30 mm thickness and Ogden material was also tested. Results presented in Fig. 7, showed that the modified TST and original THUMS model with Ogden material model yield good correlation (CORA Score 0-30ms: 0.928). Besides these, a comparison concerning the TST material influence on loading and kinematics is provided in Appendix B5.

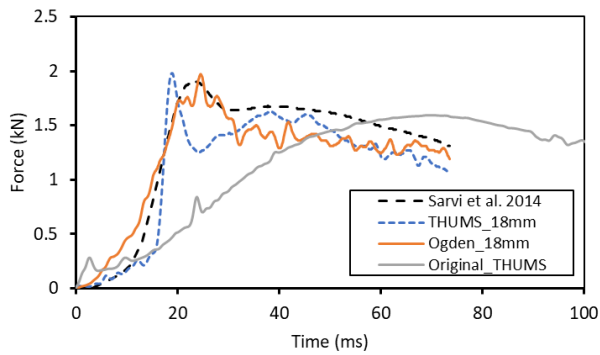


Fig. 6. The ground reaction force of the low height voluntary fall [7] vs. simulation results.

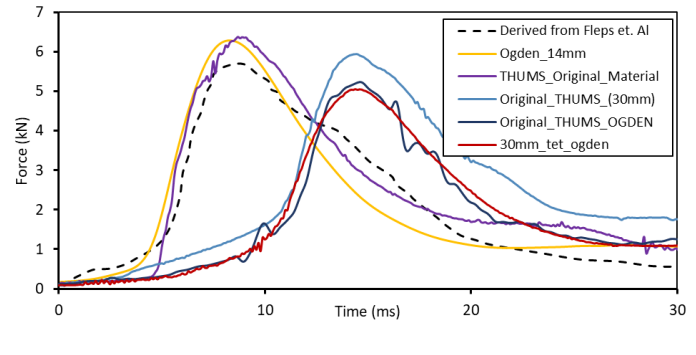


Fig. 7. Femur neck force result derived from Fleps [8] vs. simulation results

The Original THUMS V502 results, given in Fig. 6 and Fig. 7, showed a diverse impact behaviour in comparison to the reference data in both cases due to the thicker TST (30mm).

Kinematics results of both experiments are provided in Appendix D1.

Fall Simulation Results

Fall simulation results were first evaluated regarding the data inclusion criteria's; namely, only the fall configurations which yield initial hip or knee impact, and which yield normal termination for the both PID parameter sets are included. Based on this, forward-a, and backward-d (see TABLE IV) fall results were excluded. An overview of the data inclusion is provided in Appendix E. Stumbling cases were not included in the kinematic evaluations provided in this section neither. However, the corresponding stumbling results can be seen in Appendix D3. Besides these, fall kinematics of all configurations are provided in Appendix D2.

The fall simulation results showed an overall (forward, backward, lateral) average maximum vertical pelvic velocity value of 2.55 m/s and 2.34 m/s for two different PID parameter sets. The second set of PID parameters represents reduced MAs (in other words, controller reactions) and yield better agreement with the elderly falls (+6.8% error) (Fig. 8). Figure 9 exhibits the initial pelvic fall height distributions for simulation results and the published elderly falls (measured from the anterior-superior iliac spine) for comparison.

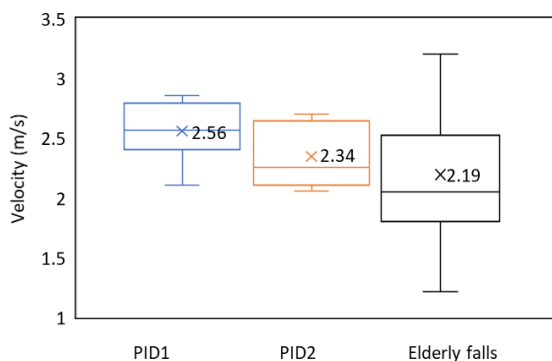


Fig. 8. Maximum vertical pelvic velocity distributions [12].

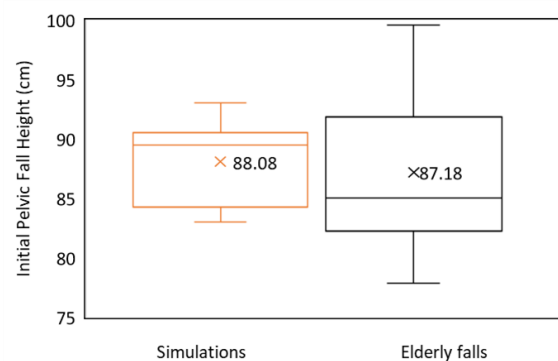


Fig. 9. Initial pelvic fall height distributions [12].

The above described elderly fall results were digitalised from Choi *et al.* [12], and cases out of the initial fall height range of 78–100 cm were excluded to avoid extremities. It should be noted that the experimental reference data include only forward and backward falls due to the reported difficulties in analysing lateral fall kinematics. However, the authors suggested that similar values could be assumed for lateral falls as well.

The results demonstrated that the horizontal pelvic velocity does not change significantly with reduced muscle activations. The median horizontal pelvic velocity at peak vertical velocity remained almost constant near 1.5 m/s (sd 0.27), while the average value was more affected by the outliers. It was reported as 1.07 m/s (sd 0.4) in elderly falls for the mentioned initial fall height range. In addition, according to the results, the protective hand contact reduced the vertical pelvis impact velocity on average, 0.06 m/s.

The trunk rotations in lateral flexed knee cases (lateral c-d, see table IV) caused an anterior or posterior pelvic impact. It is observed that the main reason for such motion was the initial knee and feet orientation (see Appendix D2). Since the feet position defines the base of support, it affected the fall kinematics substantially.

Impact results

In this section, the impact simulation results, which have been generated among the fall simulations based on the criteria mentioned in methods, are presented. An overview of the impact simulations and the kinematic results are provided in Appendix E and D, respectively. Some of the impact simulations were terminated with excessive element deformations and out of range forces. Since these numerical issues occurred during the latter part of the simulations due to upper body impact, they did not influence the hip impact evaluations. The termination status of each impact simulation is provided in Appendix D2.

The distribution of the fall-induced maximum femoral neck (FN), co-lateral FN, and fifth lumbar vertebrae (L5) forces along with the maximum FN moments for all impact simulations are given in Fig. 10. The segmental angle distributions at the instant of impact are shown in Fig. 11.

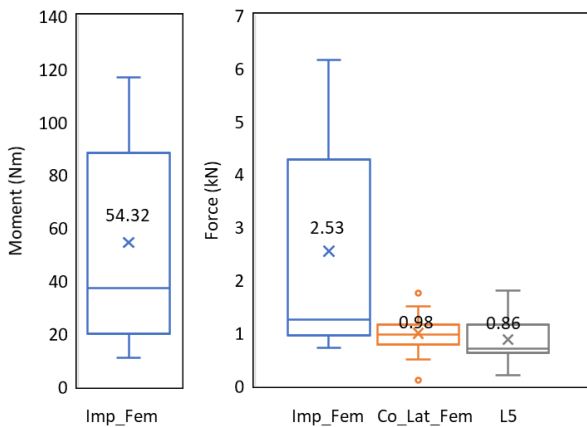


Fig. 10. Impact loading of impact side femur (Imp_Fem), co-lateral femur (Co_Lat_Fem) and fifth lumbar vertebrae (L5).

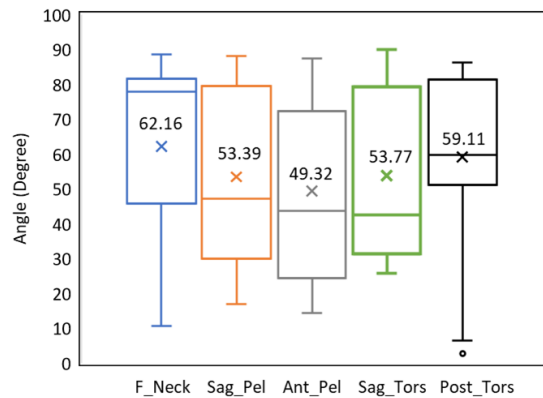


Fig. 11. Segmental angles at the instant of impact (femur neck: F_Neck, sagittal pelvic: Sag_Pel, anterior pelvic: Ant_Pel, sagittal torso: Sag_Tors and posterior torso planes: Post_Tors).

The results showed that the median FN force stayed below the reported median femoral strength value of 3.46 kN [5]. The impact configurations of the critical FN forces (above the median femoral strength) showed a particular range of segmental alignments, which caused an impact with the lateral aspect of the pelvis. The observed average segmental angles for such lateral falls were 81.1 (80.0°-84.4°), 25.8 (16.9°-31.2°), 77.2 (87.4°-71.9°), 31.16 (25.8°-37.3°) and 82.8 (86.2°-77.5°) degrees for the femur neck, sagittal pelvic, anterior pelvic, sagittal torso, and posterior torso planes, respectively.

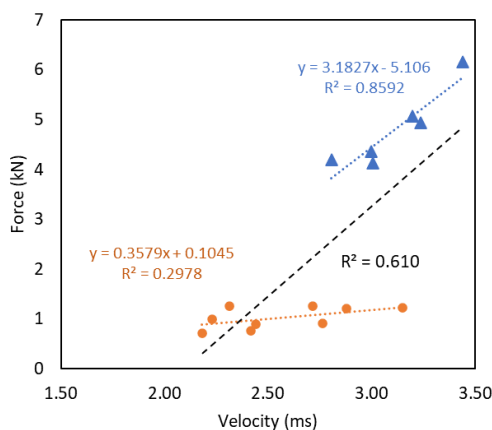


Fig. 12. Maximum FN forces vs. Maximum vertical pelvic velocities.

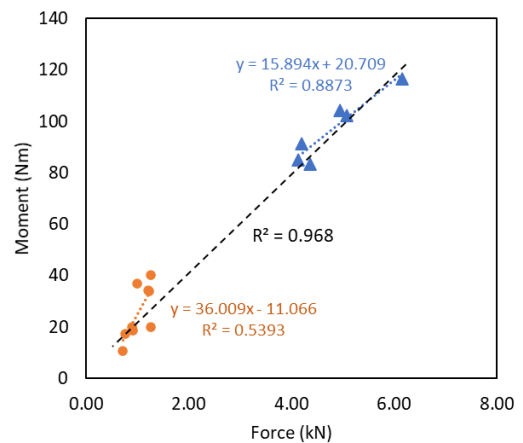


Fig. 13. Maximum FN forces vs. Corresponding FN moments.

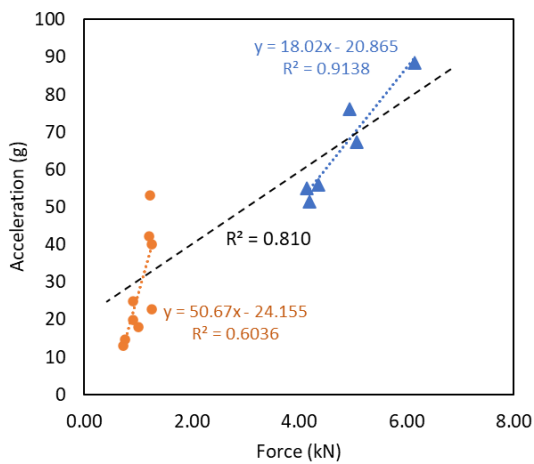


Fig. 14. Maximum vertical pelvic accelerations vs. FN forces.

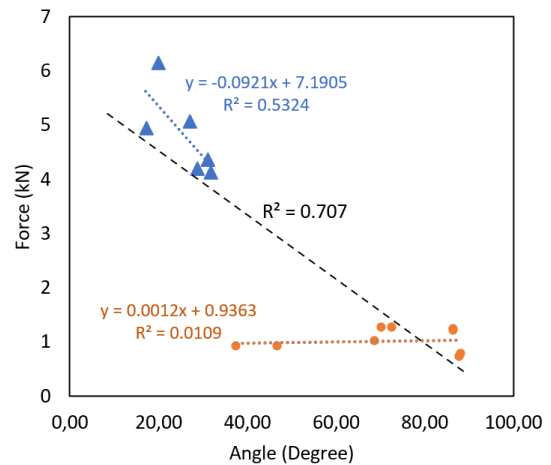


Fig. 15. Maximum FN forces vs. Corresponding Sagittal pelvis angles.

A correlation analysis was conducted to understand the association between impact parameters. The result revealed considerable correlations between the FN force - impact velocity, FN force - FN moments, pelvic acceleration - FN force, and FN force - sagittal pelvic angle. Detailed analysis of these parameters is presented in Figs 12, 13, 14, and 15, respectively. In all plots, critical lateral falls are highlighted using triangle markers. Figures show the group-specific (critical vs. others) linear regression results, as well as the coefficient of determination for linear regression of all samples.

The results yielded an average maximum head velocity of 7.13 m/s following the hip impact. This value is substantially higher than the average maximum head velocity of 4.1 m/s reported in the elderly falls [12]. The reason for this difference was the pendulum movement of the head, which in this case occurred in the absence of protective muscle activation, subsequently to the hip impact.

Influence of the muscles contractions during and after the initial impact

Fig. 16, and Fig. 17 show the peak FN force and moment results for the lateral fall induced impacts (see Appendix E) and muscle co-contractions, as described in methods. Apart from the internal-external rotator co-contractions, all patterns yielded a significant increase in the FN forces. On the contrary, the results showed significant FN moment reduction for the full contraction as well as the flexion-extension and adduction-abduction muscle co-contractions, suggesting that the muscle co-contractions could decrease the FN fracture risk.

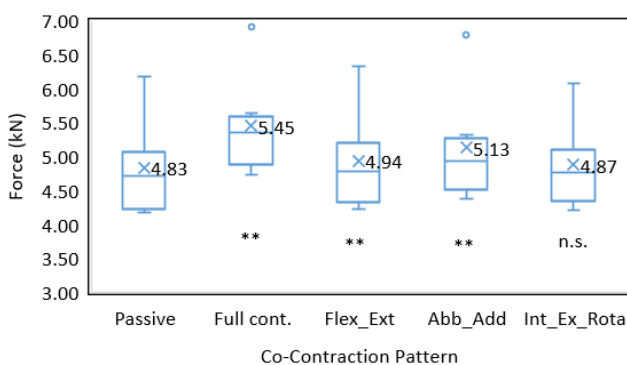


Fig. 16. Femur neck force variations in different (co-)contraction patterns (**, $p < 0.05$; n.s: Not Sign.).

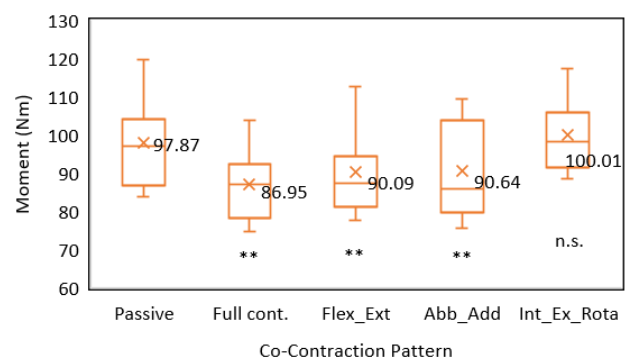


Fig. 17. Femur neck moment variations in different (co-)contraction patterns (**, $p < 0.05$; n.s: Not Sign.).

Regarding the protective muscle activations (MAs), Fig. 18 demonstrates the variation in fall kinematics with respect to the thigh, trunk and neck flexions, as mentioned in methods before, in a backward fall from standing height (Backward-d see TABLE IV). The comparison showed head velocity reduction with MAs (at 200ms 5.8m/s vs. 3.4m/s) following the hip impact such that the head velocity increased without MAs and decreased with protective flexions. Supporting the validity of this result, a similar conclusion has been drawn in the voluntary backward falls from standing height with and without protective flexions (excluding the hip flexions) [32].

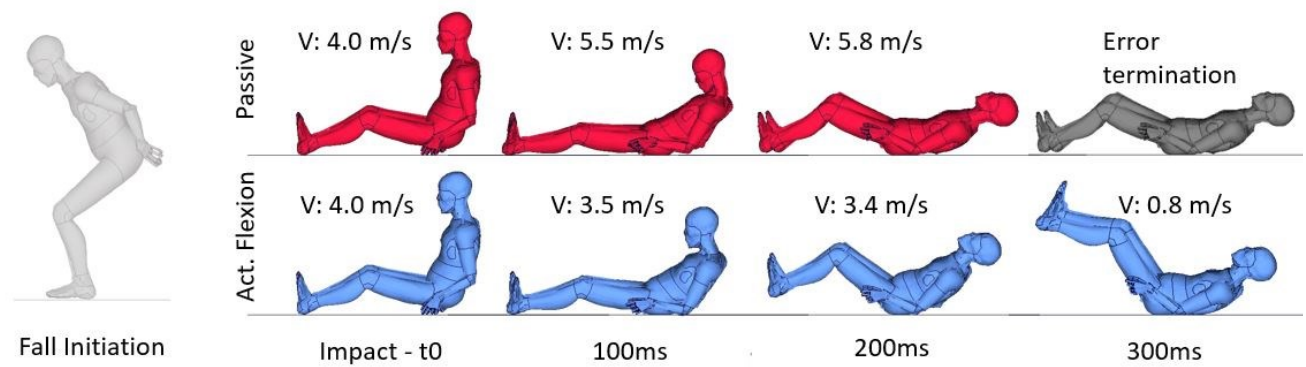


Fig. 18. Fall kinematics and head velocity change due to the protective flexions following the hip impact. (V stands for head velocity)

IV. DISCUSSION

To the best of the authors' knowledge, this is the first study that focuses on falls from standing height using HBMs and that takes into account the whole-body fall kinematics along with the muscle contractions. In addition, this approach allows us to avoid rigid constraints and boundary conditions.

In general, FE analysis is considered a more appropriate tool for fracture risk assessments than conventional clinical evaluation methods such as bone mineral density measures or fracture risk assessment tool (FRAX). However, the reliability of the FE analysis is limited to the accuracy of the applied loading and boundary conditions. To this end, detailed consideration of anthropometric parameters, fall directions, initial conditions leading to the fall, pre-impact body configuration and muscle activations (MAs) are some of the decisive parameters [5]. The main goal of this study was to show whether HBMs can address those aspects and enable detailed fall-induced femur neck (FN) force assessments.

The musculoskeletal model performance was tested in the squat and flexed standing postures using the muscle controller (MC) strategy described in methods. In squatting case, the quadriceps forces and the gluteus-maximus MA levels, as well as the joint reaction forces, are compared with the available literature. The flexed standing case was only compared against the joint reaction force ranges. Results showed that the used MC strategy provides plausible musculoskeletal forces (in physiological ranges) by sustaining the standing postures.

The impact behaviour of the models was tested and verified against relevant studies. However, the presented results do not exhibit deterministic comparisons between the model behaviour and the referenced studies. The reason for this was the subject-specific differences between the model and the corresponding person or specimen and the differences between the experimental setup and the simulations (i.e. specimen vs. whole body). However, despite those limitations, the anthropometric similarities between the models and references person or the specimen, along with the acceptable agreement of the results (low fall height with voluntaries: CORA score: 0.84; fall from standing height with the ex-vivo experiment: +10% peak error, CORA Score: 0.671, TST force drop error: +9%) support the initial validity of the modified models for LEI cases.

It should be denoted that the reference curve, used for the result comparison with ex-vivo experiment, derived from the specimen specific FE model presented by Fleps *et al.* [8] (which uses similar bone material properties as in this study). Despite the comparable ground reaction peaks (+5% error), the experimental result showed an instant force drop unlike the simulation results presented by Fleps *et al.* and in our study, suggesting that there might be fracture relevant deformations which the simulations could not capture. To this end, bone material modelling requires further attention.

The published average fall velocity of the elderly is clearly lower than the values commonly suggested [5] based on the inverse pendulum and voluntary fall experiments [33]. Our results showed that using the provided MC strategy, THUMS V502 yields 6.8% error (+0.15 m/s) in terms of the average maximum vertical pelvic velocity with the reported elderly fall velocities [12]. Besides that, the median horizontal pelvic velocity at the peak vertical velocity showed a similar trend; however, with a higher error rate (+40%) with real-life falls.

Previous literature, predicts fall kinematics and the impact forces using simplified kinematic chains with calibrated joint stiffness or PID controlled joint torques [13][20]. Considering the above mentioned plausible musculoskeletal model performance and the fall kinematics, simulating falls with PID controlled muscle activations can be considered as a contribution to the literature. Additionally, this the first study which compares model predictions with the real-life falls. The muscle control strategy presented in this work can also be calibrated

for individual fall configurations to increase the configuration-specific accuracy such as focusing only the forward, lateral or backward falls.

In terms of the FN loads, the results were mainly clustered into two groups. The first group, which had higher FN loads, consists only of the lateral pelvic impacts, as often mentioned in literature [5]. The second group, the remaining cases, includes lateral falls with posterior or anterior pelvic impacts due to the trunk rotations during the descent phase. Considering these observations, and as suggested by previous publications [34] as well, active trunk rotation strategies can be an effective method to avoid hip fractures.

Our results showed co-lateral femoral neck and lumbar spine forces up to 2 kN and 2.37 kN, respectively (Fig. 10). These values should be considered in modelling and ex-vivo studies to evaluate the limitations associated with introduced simplifications such as isolated femur or pelvic complex. Besides that, the correlation analysis revealed that the FN force and moment are correlated with the pelvic acceleration and sagittal pelvic orientation. Considering this, 3-axial pelvic acceleration measurements, which would allow monitoring both the acceleration and orientation of the pelvis, might be useful for the fall detection systems.

2 stumbling scenarios were tested based on a lateral fall from standing height (lateral-a, see TABLE IV) with 0.5 m/s anterior initial velocity using a 5cm high obstacle in 0 and 45 orientations. Results showed, in comparison to the basis lateral fall without stumbling, increased FN forces along with the higher vertical and horizontal hip impact velocities in both cases, as presented in Appendix D3.

Hip muscles are assumed to play a decisive role in joint stability and femoral stress state during the impact [25]. In order to test this hypothesis, predefined hip muscle co-contraction of the extension-flexion, adduction-abduction and internal-external-rotation muscle groups (provided in Appendix B6) were tested. Low height voluntary fall experiments have shown that the pelvic-ground reaction forces increase with the MAs due to the increased pelvic stiffness [35], assuming that the FN forces increase proportionally as well. Although the ground reaction forces did not change significantly due to the MAs in our results (probably due to increased fall height and the force levels), the FN force results presented in this study yield an increasing trend as well. However, our results also showed that even weak muscle co-contractions (activation level: 0.2) could alter the internal force transfer and reduce the FN moments, which could decrease the injury risk. A similar conclusion was also drawn in reverse pendulum experiments presented by Choi and colleagues [26]. Their results showed that while the ground reaction forces remained the same, with increasing muscle tension, normal FN forces increased, and the FN moments decreased.

There are also some limitations to this study that must be mentioned. The number of test cases for impact behaviour and musculoskeletal model performance poses an important limitation. Further validation of the models against relevant experimental data would increase the reliability of the results for the future. It is also essential to bear in mind that there is no available data to compare the complete fall kinematics with elderly falls in terms of the trajectories. Therefore, in this study, kinematic comparisons are provided only regarding the average maximum velocities, as it was given in the literature.

Although HMBs pose an advanced framework to investigate fall kinematics, impact forces and, eventually, fracture probabilities fall-specific aspects, which can vary substantially in each fall (such as the initial fall configuration, environment, ground friction etc.), still limit the general prediction capability. Therefore, the accuracy of our results is limited to the definition of fall scenarios. In terms of the generic hip fracture assessments, this limitation can be eliminated with a comprehensive statistical analysis of the fall observations. Results can be used to specify the patient group-specific fall scenarios, which would eventually allow us to define more specific femoral load cases for various patient profiles.

The calibrated TST modelling strategy was applied to whole pelvic soft tissue. However, further experimental data are required in order to support the validity of the material properties for backward falls. Besides that, a more advanced strategy would be to model adipose and muscle tissue separately accounting the subject-specific tissue thicknesses.

The impact behaviour of the upper extremities requires further verification in fall arresting cases (such as lateral-b, see TABLE IV). Results showed large shoulder and elbow deformations due to the impact loads which should be compared against the relevant experimental data. Since those deformations are more related to late impact phase (where i.e. head kinematic could be altered), it did not influence our result concerning the proximal femur loads which reach its peak value in early impact phase (0-50ms).

The simulation results are sensitive to initial conditions, such that a slight variation of the initial posture can cause diverse fall orientations. Mainly through the limited deformability of feet and ankles, the initial foot angles largely vary the base of support and, therefore, the fall orientation (see lateral-c and -d in Appendix D2). For this reason, biofidelic foot models would improve model performance.

The MAs initially were not considered in impact simulations. The main reason for this was, the missing evidence in the literature regarding MAs at the instance of a fall induced impact. Considering the time range of the hip impacts (20-50ms), we eliminated the MAs in initial fall simulations in order to avoid misleading influences. In these simulations, however, the late impact head kinematic is disadvantaged by this decision. Without the MAs, the simulation results yielded higher head velocities than the observed values in the elderly falls (7.3 vs 4.1 m/s) [12]. In order to address this problem, a protective flexion strategy was tested in a particular backward fall configuration (backward-d, see TABLE IV). The results provided a related head velocity reduction (3.2 m/s vs 4.25m/s) with the voluntary fall experiments [32].

The muscle control strategy presented in this work provided plausible results in terms of the fall kinematics and the musculoskeletal forces. However, from a neuromuscular point of view, PID control can be considered a primitive method to represent complex motion and muscle synergy patterns. In conventional neuromuscular modelling, widely used for various research purposes [36-37], MA is mainly determined based on the energy minimisation principle for defined motion patterns. However, this approach is only valid for a controlled neuromuscular state and cannot be used for fall events. In order to predict the MAs more realistically, further research is required to develop a neuromuscular objective function for fall events.

In this work, the target joint angle offsets (TJAOs) and PID gains are calibrated to sustain standing postures as mentioned in methods. Initially, the same MC parameters are used in fall configurations by adjusting the upper body MA directions to enable fall opposite (protective) bending. Later PID parameters were varied to adjust the fall kinematics. In this study, the target joint angles (JAs) kept constant during the falls, which pose a major limitation since the MAs should vary following the postural shift. For instance, it could be expected that the co-lateral leg and hip undergo unrealistic extension with the changing body inclination in lateral falls. However, fall simulations showed on average plausible fall kinematic (+6.8% pelvic velocity error) and extremity motions since the time range of the falls were rather short to generate such excessive motions. Besides that, no motion or MA patterns were defined for upper extremities. However, in real-life, a subject would move the upper extremities to recover the balance [33] (if not avoidable, arrest the fall), by shifting the body weight. Additionally, upper extremity movements may increase the upper body moment of inertia. Such motion could affect the presented results in terms of the fall duration and fall kinematic, as well as the segmental angle orientation, maximum pelvic velocity and FN loading.

The published real-life forward fall kinematics are highly related to preventing stepping, such that forward falls from standing height do not occur without preventive stepping, and show high horizontal velocities [12]. As mentioned above, the MC strategy presented in this study was not able to generate such coordinated movements. Therefore, in these fall configurations, the predicting power of our models is limited in terms of the fall kinematics. Due to this limitation, forward fall simulation result without flexed knee (forward-a, see TABLE IV) yield unrealistic behaviour (initial head impact) and excluded from evaluations.

In the future, the above-mentioned limitations of the MC can be eliminated to some extent defining functional or time-dependent target JAs. Using a simplified model, the MC parameters can be calibrated for the desired musculoskeletal performance and later applied to the full-scale model.

The femoral stress state needs to be evaluated in detail to understand the influence of the muscle contractions in terms of the femur fracture risk. Here, a comprehensive analysis is not provided since it was beyond the focus of this work.

In this study, anthropomorphic variations were not considered. It is expected that fall kinematics, and the impact behaviour will be influenced by the anthropometric variations, and therefore they require further attention in the future. Bone fracture was not considered either. Patient-specific bone modelling, including fracture properties, would also increase the model accuracy.

V. CONCLUSIONS

The primary purpose of this study was to investigate the LEI-induced femur neck loads using HBMs. Based on our findings, the following conclusions can be drawn:

- following the described trochanteric soft tissue modelling modifications, THUMS V502 provides plausible impact forces in LEIs;
- regarding the fall kinematics, the presented muscle control strategy showed similar average vertical pelvic velocity results with the real-life observations.

- the fall-induced FN forces above the median femur strength are associated with a specific arrangement of segmental orientations and can be correlated with the vertical pelvic impact velocity, sagittal pelvic angle, and pelvic acceleration;
- the hip muscle co-contractions can reduce the FN moment during the impact.

In summary, THUMS V502 enables a detailed investigation of LEI-induced femur neck loads, including plausible fall kinematics, impact behaviour and muscle activations. Our study presented an initial effort towards comprehensive low energy fall simulations using HBMs. Eliminating the limitations, we believe, similar models hold great potential to help researchers to gain a greater understanding of LEIs and to develop strategies to reduce injury risks.

VI. ACKNOWLEDGEMENT

We would like to thank Ingenieurgesellschaft für Automobiltechnik mbH and Julius-Wolff-Institute for facilitating this work and Prof. Duane Cronin for his valuable comments and support. We also acknowledge the guiding comments of Dr Adam Trepczynski, Dr Mark Heyland and Dr Philipp Damm.

VII. REFERENCES

- [1] Dhanwal, D. K., Dennison, E. M., Harvey, N. C., Cooper, C. (2011) Epidemiology of hip fracture: Worldwide geographic variation. *Indian journal of Orthopaedics*, **45**(1): pp.15–22.
- [2] Magaziner, J., Fredman, L., et al. (2003) Changes in functional status attributable to hip fracture: a comparison of hip fracture patients to community-dwelling aged. *American journal of epidemiology*, **157**(11): pp.1023–1031.
- [3] Luo, Y. (2016) A biomechanical sorting of clinical risk factors affecting osteoporotic hip fracture. *Osteoporosis international*, **27**(2): pp.423–439.
- [4] Kanis, J. A., Oden, A., et al. (2009) FRAX and its applications to clinical practice. *Bone*, **44**(5): pp.734–743.
- [5] Sarvi, M. N.; Luo, Y. (2017) Sideways fall-induced impact force and its effect on hip fracture risk: a review. *Osteoporosis international*, **28**(10): pp.2759–2780.
- [6] Kroonenberg, A. J., Hayes, W. C., McMahon, T. A. (1996) Hip impact velocities and body configurations for voluntary falls from standing height. *Journal of Biomechanics*, **29**(6): pp.807–811.
- [7] Sarvi, M. N., Luo, Y., Sun, P., Ouyang, J. (2014) Experimental Validation of Subject-Specific Dynamics Model for Predicting Impact Force in Sideways Fall. *Journal of Biomedical Science and Engineering*, **07**(07): pp.405–418.
- [8] Fleps, I., Guy, P., Ferguson, S. J., Crompton, P. A., Helgason, B. (2019) Explicit Finite Element Models Accurately Predict Subject-Specific and Velocity-Dependent Kinetics of Sideways Fall Impact. *Journal of bone and mineral research*, **34**(10): pp.1837–1850.
- [9] Zani, L., Erani, P., Grassi, L., Taddei, F., Cristofolini, L. (2015) Strain distribution in the proximal Human femur during in vitro simulated sideways fall. *Journal of Biomechanics*, **48**(10): pp.2130–2143.
- [10] Robinovitch, S. N., Feldman, F., et al. (2013) Video capture of the circumstances of falls in elderly people residing in long-term care: an observational study. *The Lancet*, **381**(9860): pp.47–54.
- [11] Yang, Y., van Schooten, K. S., et al. (2018) Sex Differences in the Circumstances Leading to Falls: Evidence From Real-Life Falls Captured on Video in Long-Term Care. *Journal of the American Medical Directors Association*, **19**(2): pp.130-135.e1.
- [12] Choi, W. J., Wakeling, J. M., Robinovitch, S. N. (2015) Kinematic analysis of video-captured falls experienced by older adults in long-term care. *Journal of Biomechanics*, **48**(6): pp.911–920.
- [13] Lo, J.; Ashton-Miller, J. A. (2008) Effect of pre-impact movement strategies on the impact forces resulting from a lateral fall. *Journal of Biomechanics*, **41**(9): pp.1969–1977.
- [14] Toyota Motor Company (2016) Total Human Model for Safety AM50 Occupant Model Version 5.02 Documentation

- [15] Livermore Software Technology Corporation (2016) Ls-Dyna R9.0® Keyword User's Manual Volume I .
- [16] El-Sherbiny, Y. M., Hasouna, A. T., Ali, W. Y. (2012) Friction coefficient of rubber sliding against flooring materials. *Asian Research Publishing Network Journal of Engineering and Applied Sciences*, **7**: pp.121–126.
- [17] Ramalho, A., Szekeres, P., Fernandes, E. (2013) Friction and tactile perception of textile fabrics. *Tribology International*, **63**: pp.29–33.
- [18] ProHMSiG, <https://www.iatmbh.com/methoden-prozesse/prohmsig/> . [Accessed 25.03.2020].
- [19] OrthoLoad public data base, <https://orthoload.com/database/> . [Accessed 01.06.2020].
- [20] Luo, Y.; Sarvi, M. N. (2015) A subject-specific inverse-dynamics approach for estimating joint stiffness in sideways fall. *International Journal of Experimental and Computational Biomechanics*, **3**(2).
- [21] Fleps, I., Vuille, M., et al. (2018) A novel sideways fall simulator to study hip fractures ex vivo. *PloS one*, **13**(7): pp.1–15.
- [22] Fleps, I., Enns-Bray, W. S., et al. (2018) On the internal reaction forces, energy absorption, and fracture in the hip during simulated sideways fall impact. *PloS one*, **13**(8): pp.e0200952.
- [23] Levine, I. C., Minty, L. E., Laing, A. C. (2015) Factors that influence soft tissue thickness over the greater trochanter: application to understanding hip fractures. *Clinical anatomy (New York, N.Y.)*, **28**(2): pp.253–261.
- [24] Karajan, N., Fressmann, D., Erhart, T., Schumacher, P. (2013) Biomechanical Material Models in Ls-Dyna.
- [25] Retchford, T. H., Crossley, K. M., Grimaldi, A., Kemp, J. L., Cowan, S. M. (2012) Can local muscles augment stability in the hip? A narrative literature review. *Journal of Musculoskeletal And Neuronal Interactions*, (13): pp.1–12.
- [26] Choi, W. J.; Robinovitch, S. N. (2018) Effect of pelvis impact angle on stresses at the femoral neck during falls. *Journal of Biomechanics*, **74**: pp.41–49.
- [27] Kleinberger, M., Sun, E., Eppinger, R., Kuppa, S., Saul, R. (1998) Development of Improved Injury Criteria for the Assessment of Advanced Automotive Restraint Systems. *National Highway Traffic Safety Administration*.
- [28] Objective rating metric for non-ambiguous signals, <https://www.iso.org/obp/ui/#iso:std:iso:ts:18571:ed-1:v1:en> . [Accessed 03.06.2020].
- [29] Dahlkvist, N. J., Mayo, P., Seedhom, B. B. (1982) Forces during Squatting and Rising from a Deep Squat. *Engineering in Medicine*, **11**(2): pp.69–76.
- [30] Williams, M., Gibson, N., et al. (2018) Activation of the Gluteus Maximus During Performance of the Back Squat, Split Squat, and Barbell Hip Thrust and the Relationship With Maximal Sprinting. *Journal of Strength and Conditioning Research*: pp.1–9.
- [31] Robinovitch, S. N., McMahan, T. A., Hayes, W. C. (1995) Force attenuation in trochanteric soft tissues during impact from a fall. *Journal of Orthopaedic Research*, **13**(6): pp.956–962.
- [32] Choi, W. J., Robinovitch, S. N., Ross, S. A., Phan, J., Cipriani, D. (2017) Effect of neck flexor muscle activation on impact velocity of the head during backward falls in young adults. *Clinical biomechanics (Bristol, Avon)*, **49**: pp.28–33.
- [33] Feldman, F., Robinovitch, S. N. (2007) Reducing hip fracture risk during sideways falls: evidence in young adults of the protective effects of impact to the hands and stepping. *Journal of Biomechanics*, **40**(12): pp.2612–2618.
- [34] Robinovitch, S. N., Inkster, L., Maurer, J., Warnick, B. (2003) Strategies for Avoiding Hip Impact During Sideways Falls. *Journal of bone and mineral research*(18).
- [35] Martel, D. R., Levine, I. C., Pretty, S. P., Laing, A. C. (2018) The influence of muscle activation on impact dynamics during lateral falls on the hip. *Journal of Biomechanics*, **66**: pp.111–118.
- [36] Seth, A., Hicks, J. L., et al. (2018) OpenSim: Simulating musculoskeletal dynamics and neuromuscular control to study human and animal movement. *PLOS Computational Biology*, **14**(7): pp.e1006223.

[37] AnyBody Technology Inc. AnyBody Publications, <https://www.anybodytech.com/downloads/publications/>. [Accessed 25.03.2020].

[38] Erhart, T. (2011) Review of Solid Element Formulations in Ls-Dyna. Dynamore GmbH

VIII. APPENDIX

Appendix A) – Positions

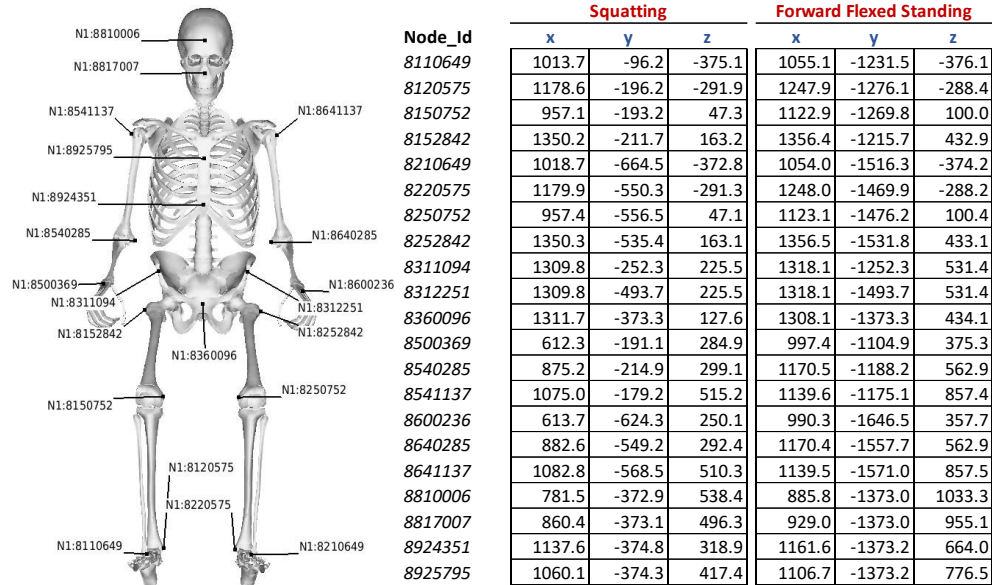


Fig. A1. Squatting and forward flexed standing posture nodal coordinates

	Forward-a			Forward-b			Lateral-a			Lateral-b			Lateral-c		
	x	y	z	x	y	z	x	y	z	x	y	z	x	y	z
Neck	-	3	-	-	3	-	-	-	-	-	5	-	-	-	-
Torso	-	5	-	-	5	-	3	-	7	-	3	22	3	-	7
Hip Left	-	10	-	-	11	4	-	5	-	-	5	-	9	10	5
Hip Right	-	10	-	-	11	-5	-9	-	-4	-9	-	-3	17	4	33
Knee Left	-	-	-	-	26	-	-	-	-	-	-	-	-	5	-
Knee Right	-	-	-	-	26	-	-	-	-	-	-	-	-	26	-
Ankle Right	-	-11	-	4	-22	4	-	-	-	-	-	-	-	-7	-
Ankle Left	-	-11	-	-3	-23	-	-	-	-	-	-	-	-5	-27	-3
Scapula-Thorax Right	-	-	-	-	-	-	-	-	-	-	9	-	-	-	-
Scapula-Thorax Left	-	-	-	-	-	-	-	-	-	-6	3	-	-	-	-
Shoulder Right	-	-36	-4	-3	-37	-4	-4	-11	-10	7	-20	10	-16	-10	4
Shoulder Left	-	-36	4	3	-37	4	-	-6	-11	-7	17	54	-3	-5	-12
Elbow right	-	-	-	-	-	-	16	24	20	43	-19	-16	32	19	6
Elbow Left	-	-	-	-	-	-	6	-36	10	8	8	-31	7	-34	10
Wrist Right	-	-	-	-	-	-	-7	-	-	9	23	3	-6	10	-
Wrist Left	-	-	-	-	-	-	-6	6	-	-8	-8	-5	-5	6	-

	Lateral-d			Bacward-a			Backward-b			Backward-c			Bacward-d		
	x	y	z	x	y	z	x	y	z	x	y	z	x	y	z
Neck	-	-	5	-	-	-	-	-	-	-	-	-	-	-	-
Torso	-	3	21	-	-	-	-	-	-	-	-	-	-	-	-
Hip Left	9	11	-	-	-3	-	-	-	-	-	-19	-	-	-19	-
Hip Right	20	4	30	-	-3	-	-	-	-	-	-19	-	-	-19	-
Knee Left	-	4	-	-	4	-	-	-	-	-	20	-	-	20	-
Knee Right	-	26	-	-	4	-	-	-	-	-	20	-	-	20	-
Ankle Right	-	-6	-	-	5	-	-	7	-	-	-8	-	-	-7	3
Ankle Left	-6	-27	-	-	5	-	-	7	-	-	-8	-	-	-8	-
Scapula-Thorax Right	-	-	10	-	-	-	-3	3	-7	-	-	-	6	4	-4
Scapula-Thorax Left	-	-	6	-	-	-	4	4	7	-	-	-	-6	5	4
Shoulder Right	6	-22	11	-	-	-	-3	54	-15	-	-	-	-9	56	-43
Shoulder Left	-	15	31	-	-	-	5	50	20	-	-	-	9	56	44
Elbow right	39	-25	-18	-7	-6	-7	4	-6	-	-	-	-	-	-23	24
Elbow Left	-	-	3	7	-6	7	-3	-5	-4	-	-	-	-	-22	-22
Wrist Right	8	25	-	-	-	-	19	5	3	-	-	-	14	8	4
Wrist Left	-	-6	-6	-	-	-	-18	4	-3	-	-	-	-12	7	-5

Fig A2. Fall configuration joint angle deviations from the forward flexed standing posture.

Appendix B) – Impact verification and TST modelling

B1) Model positioning for voluntary falls

Figure B1 shows the positioned model based on the segmental angles given in Fig. B2. Adjusting the segmental lengths for THUMS V502 and using the segmental angles, positioning pointers, shown in Fig. B1, were generated. Since the segmental angles were determined based on the left-right average coordinates of the ankle, knee and ASIS markers on voluntary tests, pointers were used similarly to guide the model positioning. In details, the model was positioned so that the average marker coordinates align with the positioning pointer within 3 cm tolerance.

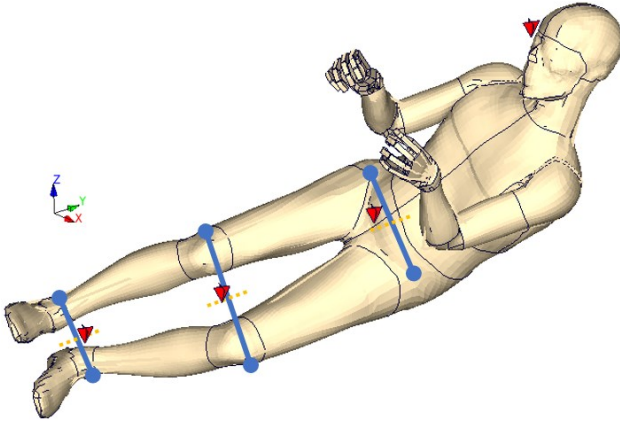


Fig. B1. Voluntary fall posture and the reference pointers

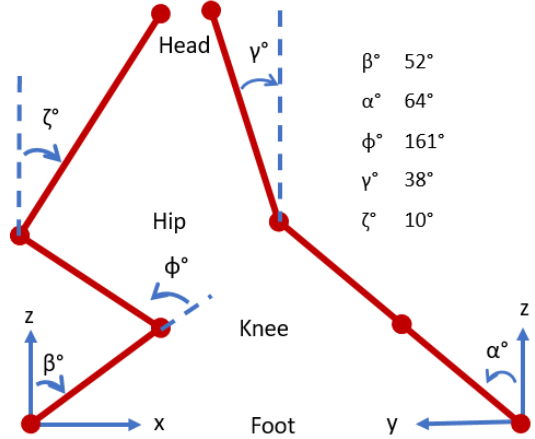


Fig. B2. Positioning data provided by Lou *et al.* [7].

It should be denoted that using the available information a deterministic positioning of all available degrees of freedoms were not possible. Additionally, due to the anthropometric differences and the uncertainties in the positioning procedure, initial fall height was higher than 5 cm. In order to ensure the right pelvic impact velocity, a rigid adjustment plate was included as described in methods. Although the uncertainties mentioned above, considering that the femur-hip-torso alignments and the fall height of the model present the reported experiment, simulation results were compared with the experimental result to evaluate the model performance.

B2) Ex-vivo falls from standing height - experimental results and model positioning

Figure B3 shows ground reaction forces (specimen H1402) for the experimental and the specimen specific simulation result presented by Fleps [8] as well as the derived FN force result. Since our simulation models use an elastoplastic bone modelling without fracture, FE model result with non-linear material properties, which yields no fracture for H1402, used as a starting reference. In another publication, based on the similar ex-vivo experiments and simulation models [22], authors showed that FN force and the ground reaction forces follow a similar trend. Therefore ground reaction force is scaled based on the reported FN peak force value using the following equation:

$$\mathbf{F}_{FN_{derived}} = \left(\frac{F_{FN_{peak}}}{F_{Gr_{peak}}} \right) * \mathbf{F}_{Gr}$$

where, $\mathbf{F}_{FN_{derived}}$ is derived FN force, $F_{FN_{peak}}$ is the FN peak value, $F_{Gr_{peak}}$ is the ground reaction peak value and the \mathbf{F}_{GR} is the ground reaction force.

The model was positioned based on segmental angles provided by the authors as supplementary material [21] (Fig. B4 and B5). In details, first, the lower extremities and the pelvis were positioned locally based on the hip flexion, knee, impacted leg-pelvis, internal rotation, and pelvis tilt angles. Finally reported pelvic rotation around the z-axis (in our case x) was applied to determine global position. Apart from the given reference angles, upper body position represents a forward flexed initial fall configuration with a straight back. Arms were positioned slightly stretched to avoid strong inertial influences. Left-arm was flexed to prevent extra load transfer during the impact.

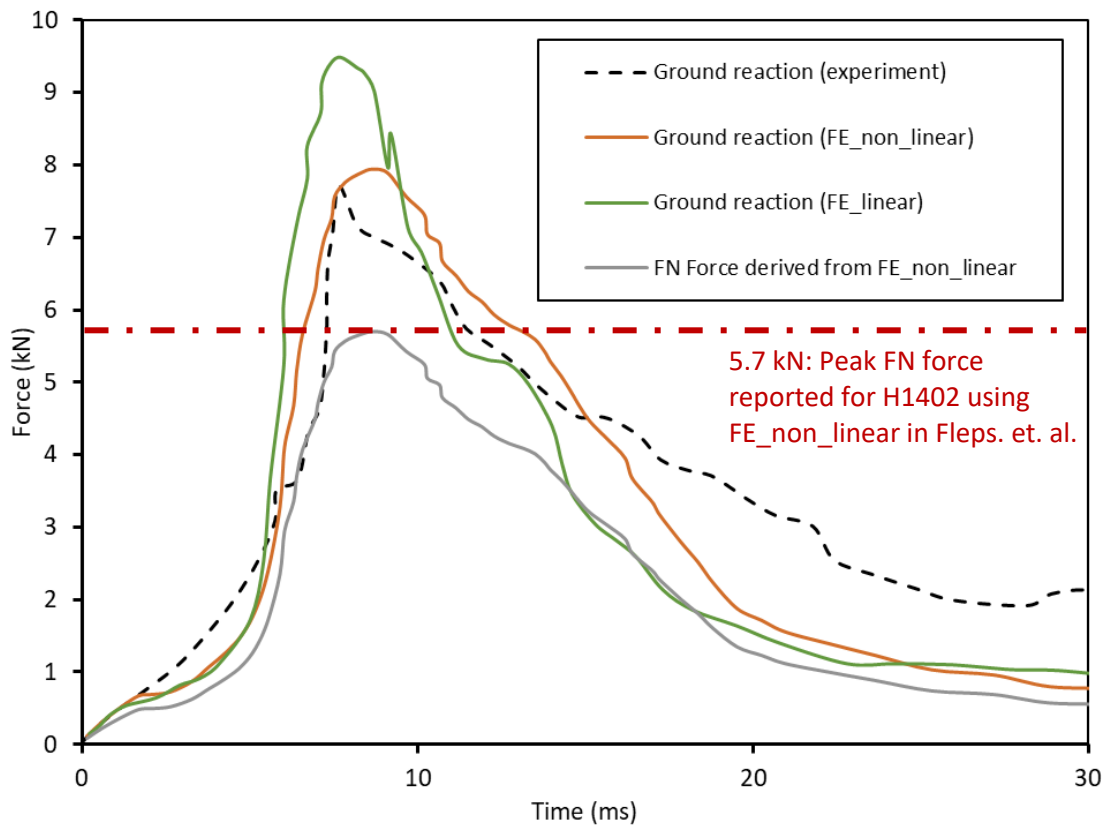


Fig. B3. Presented ex-vivo and in-silico ground reaction forces (digitalised from Fleps *et al.* [22]) and the derived FN force reference.

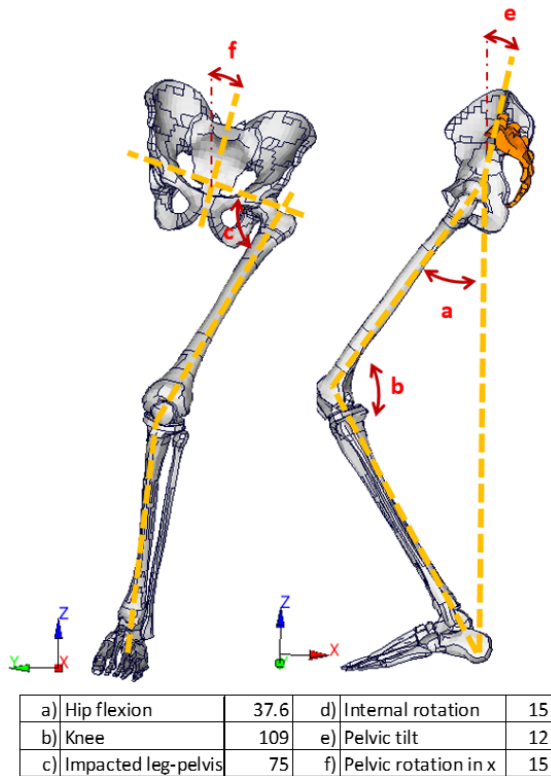


Fig. B4. Lower limb segmental angles for the ex-vivo falls

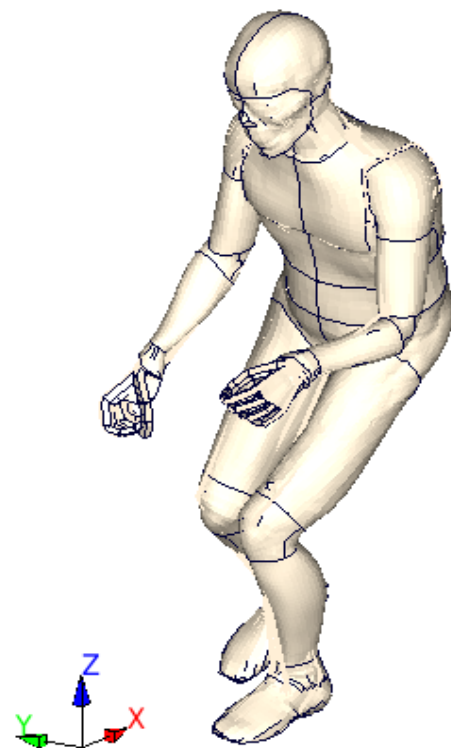


Fig. B5. Positioned model for falls from standing height

B3) Calibrated Trochanteric Soft Tissue Material

The material definition provided in Fig. B6 was manually calibrated to improve the fall induced impact behaviour, as mentioned in the Low Energy Impact Verification Section.

```
*MAT_OGDEN_RUBBER
$: mid ro pr n nv g sigf ref
1 1.0E-9 0.49 0 2 0.0 0.0 0.0
$: mu1 mu2 mu3 mu4 mu5 mu6 mu7 mu8
4.0E-2 0.0E-5 4.0E-4 2.0E-4 0.0 0.0 0.0 0.0
$: alpha1 alpha2 alpha3 alpha4 alpha5 alpha6 alpha7 alpha8
1.0 2.0 4.5 6.0 0.0 0.0 0.0 0.0
$: g1 beta1 vflag
0.2 1.0E+4 1
$: g2 beta2
3.0E-1 1.0E+2
$: g3 beta3
0.0 0.0
...
...
...
$: g12 beta12
0.0 0.0
```

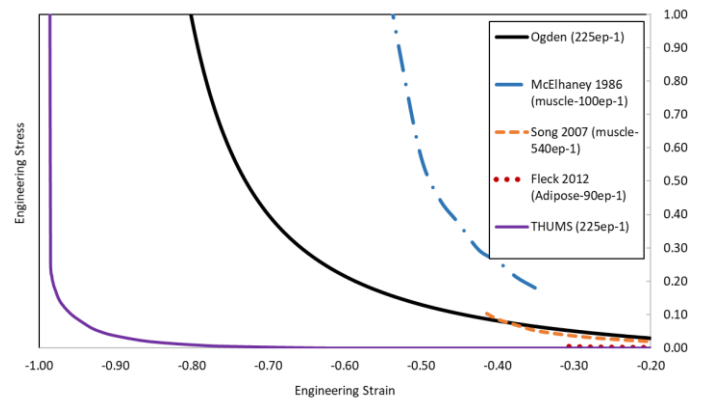


Fig. B6. Implemented Ogden material model in LS-Dyna.

Fig. B7. Literature Comparison.

The literature comparison chart (Fig. B7) shows the specimen compression test results of the calibrated material model and the relevant publications as well as the original material model used in THUMS V502 for a comparable range of strain rates. In detail, results presented by McElhaney (1986), Song (2007) and Fleck (2012) were based on the compression test results of bovine muscle in the fibre direction, porcine muscle perpendicular to fibre direction and adipose tissue, respectively. Results showed that the implemented Ogden model follows a more similar trend as the results from Song 2007 (porcine muscle perpendicular to fibre direction) while the original THUMS V502 TST material seems to be more comparable with the adipose tissue. It should also be mentioned that the strain ranges provided in experimental results do not cover the high compressive strain regions.

B4) Mesh sensitivity test results and comments on element formulation

The mesh sensitivity test was carried out based on the TST impact test presented by Robinovitch *et al.* 1995 [31]. Authors developed an experimental setup to investigate TST thickness influence over the trochanter reaction forces. In detail, cadaveric TSTs were attached to a rigid trochanter and a spring with a stiffness of 150N/mm. Later, a 44 kg mass impacted the TST with 2.5 m/s impact velocity. This setup yields similar reaction forces as observed in falls from standing height using the same impact speed and effective mass.

Since the main focus of our study is the fall-induced proximal femur loads, a similar simulation setup developed for the mesh sensitivity test. A spherical mass (44kg) was impacted on a 15 mm thick, soft tissue with different element size and formulations (Fig. B8) using the previously provided Ogden material model. On the bottom, the soft tissues were connected to a rigid plate and a discrete element which models the spring used in the reported experiment.

Simulations with hexahedral elements yield error termination due to the negative element jacobian, while the tetrahedral elements posed a more robust performance. In general, using hyperelastic material models, tetrahedral elements with 1 point nodal pressure formulation (Eq. 13) have more superior performance in comparison to default tetrahedral element due to the volumetric locking problem [38]. However, Eq. 13 tetrahedral elements require increased mesh density. In TST modelling (in our case minimum thickness is 14mm) it was challenging to sustain required element size and the surrounding mesh compatibility. Therefore, considering the close agreement (CORA score: 0.976), as shown in Fig. B9, between the default tetrahedral elements (5mm) and Eq. 13 tetrahedral elements (1mm), in this study, default tetrahedral elements were used.

Additionally, using the presented Ogden model, original THUMS model (which uses hexahedral elements) is compared with the modified model in terms of the femur neck forces in falls from standing height. Again the simulation results showed a good correlation (CORA score: 0.928) (See Impact verification results).

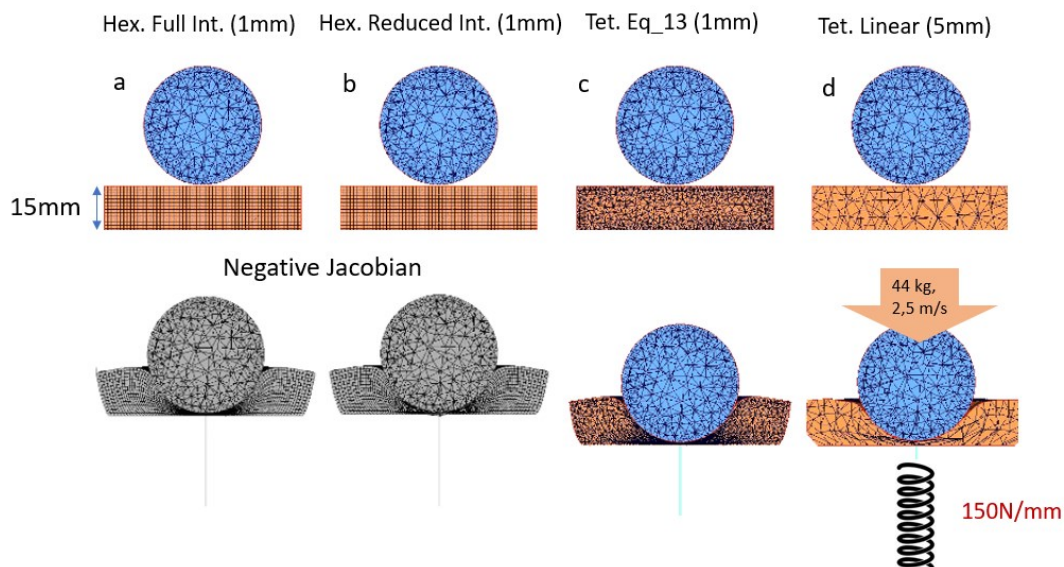


Fig. B8. Mesh sensitivity simulations: a) Full integration hexahedral elements with 1mm edge length, b) Reduced integration hexahedral elements (standard, viscous hourglass control) with 1mm edge length, c) Equation 13 (1 point nodal pressure) tetrahedral elements with 1mm edge length, d) Default (constant stress) tetrahedral elements with 5mm edge length.

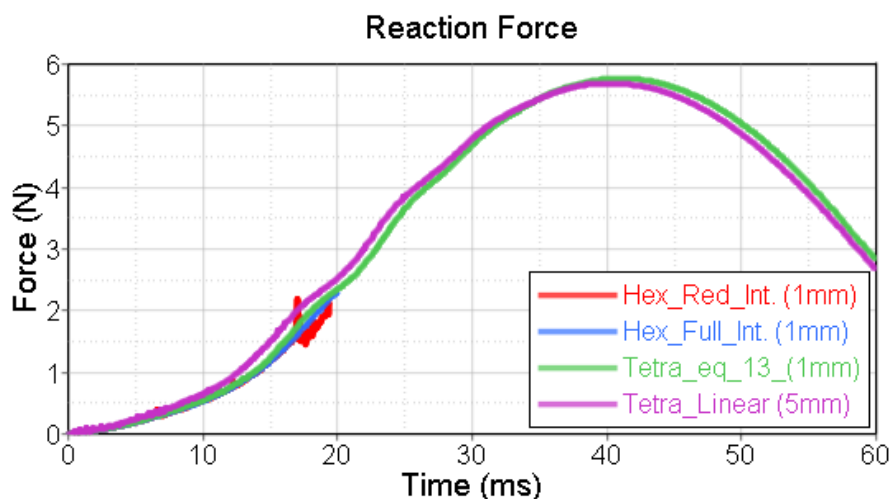


Fig. B9. Mesh sensitivity test reaction forces

B5) TST material influence on kinematic and loading

TABLE B1. shows a comparison in terms of the kinematic and loading values between the original THUMS V502 and using the implemented Ogden material model with the same model. The impact results were provided from the ex-vivo fall configuration from standing height, as presented in the Low Energy Impact Verification Section, for a time range of $t_0 + 80$ ms.

TABLE B1
MATERIAL MODEL INFLUENCE

	Max. Imp. FN (kN)	Max. Co. lat. FN (kN)	Max. L5 (kN)	Max. Pelvis Acc. (g)	Max. Head Acc. (g)
THUMS V502	5.94	1.15	0.64	71.4	0.8
with Ogden	5.05	1.15	0.6	63.7	0.8

Results showed that the changes in TST material have a higher influence on the FN loads and the pelvic acceleration in case of a TST thickness of 30mm.

B6) Left hip muscles coordination matrix

TABLE B2
MUSCLE COORDINATION MATRIX

	Flexion	Extension	Adduction	Abduction	Int. Rot.	Ext. Rot
Psoas 1-6	1.0					
Iliacus	1.0					
Piriformis		0.25		0.25		0.5
Superior-Gemellus		0.2				0.8
Inferior-Gemellus						0.8
Obturator-Externus				0.5		0.5
Obturator-Internus		0.2				0.8
Quadratus-Femoris			0.5	0.5		0.5
Gluteus_Min_L				0.8	0.2	
Gluteus_Med_L				0.8	0.2	
Gluteus_Max_1		0.7				0.3
Adductor-Brevis	0.2		0.8			
Adductor-Longus	0.2		0.8			
Adductor-Magnus		0.1	0.9			
Pectineus_L	0.1		0.9			
Tensor-Fasciae-Latae	0.35			0.35	0.3	
Rectus-Femoris	1.0					
Sartorius	0.3			0.1		0.3
Semi-Tendinosus		0.4			0.2	
Semi-Membranosus		0.4			0.2	
Gracilis	0.3			0.3	0.2	
Biceps-Femoris-Longum		0.5				

The muscle coordination matrix provided in TABLE B2 is used in muscle co-contraction investigations. It defines the activation ratios for individual muscles based on the basis activation level of the corresponding motion group. For example, in case of a basis activation signal of 0.5 for flexion, the activation level of Iliacus and Adductor-Brevis will be 0.5 and 0.1 respectively. Similarly, the activation level of the other relevant flexion muscles will be adjusted in the same manner. This principle applies to all motion groups with the following formula:

$$Act_{muscle(i)} = M_{musclecoord(ij)} Act_{motion(j)} ;$$

where, $Act_{muscle(i)}$ is muscle activation level, $M_{musclecoord(ij)}$ is muscle coordination matrix and $Act_{motion(j)}$ is the activation for the motion group.

Appendix C) – Simulation Outputs

TABLE C1 gives a summary of the used measurement methods in the simulation models. Figure C1 shows a visualisation of the segmental body planes used in impact simulation post-processing to quantify the body postures.

TABLE C1
FORCE AND ACCELERATION MEASUREMENTS

Femur Neck Loads	"DATABASE_CROSS_SECTION_PLANE" (it is placed on the middle of the FN with a parallel normal to femur neck axis)
L5 loads	"DATABASE_CROSS_SECTION_SET" (It uses the inferior elements of the vertebrae)
Pelvic Acceleration/Velocity	It is measured on the geometric centre of the pelvis. Measurement node is attached to sacrum using "CONSTRAINED_INTERPOLATION" definition.
Head acceleration/Velocity	It is measured on the centre of gravity of the head. Measurement node is attached to parietal and frontal bones using "CONSTRAINED_INTERPOLATION" definition.

Figure C1 shows the segmental planes described in Impact Simulations Section.

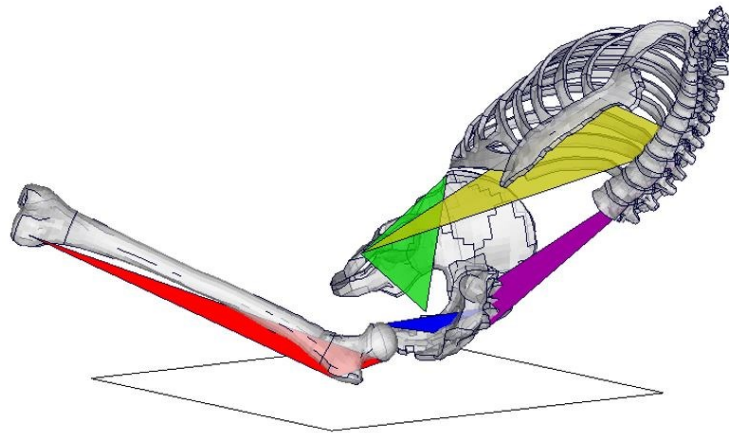


Fig. C1. Segmental planes: Femur Neck Plane (red), Sagittal Pelvic Plane (blue), Anterior Pelvic Plane (green), Sagittal Torso Plane (yellow), Posterior Torso Plane (purple)

Appendix D) – Fall and Impact Kinematics

D1) Impact verification

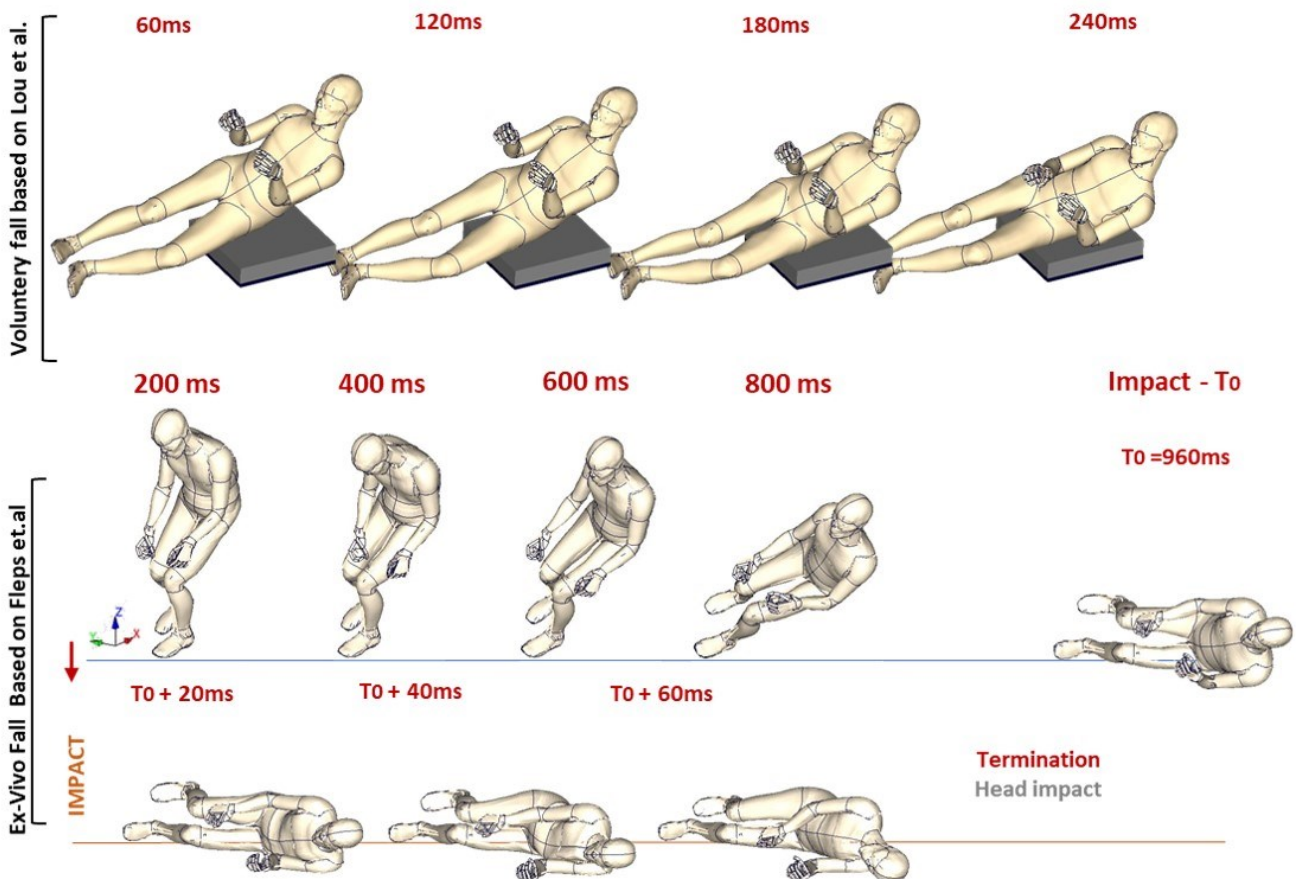
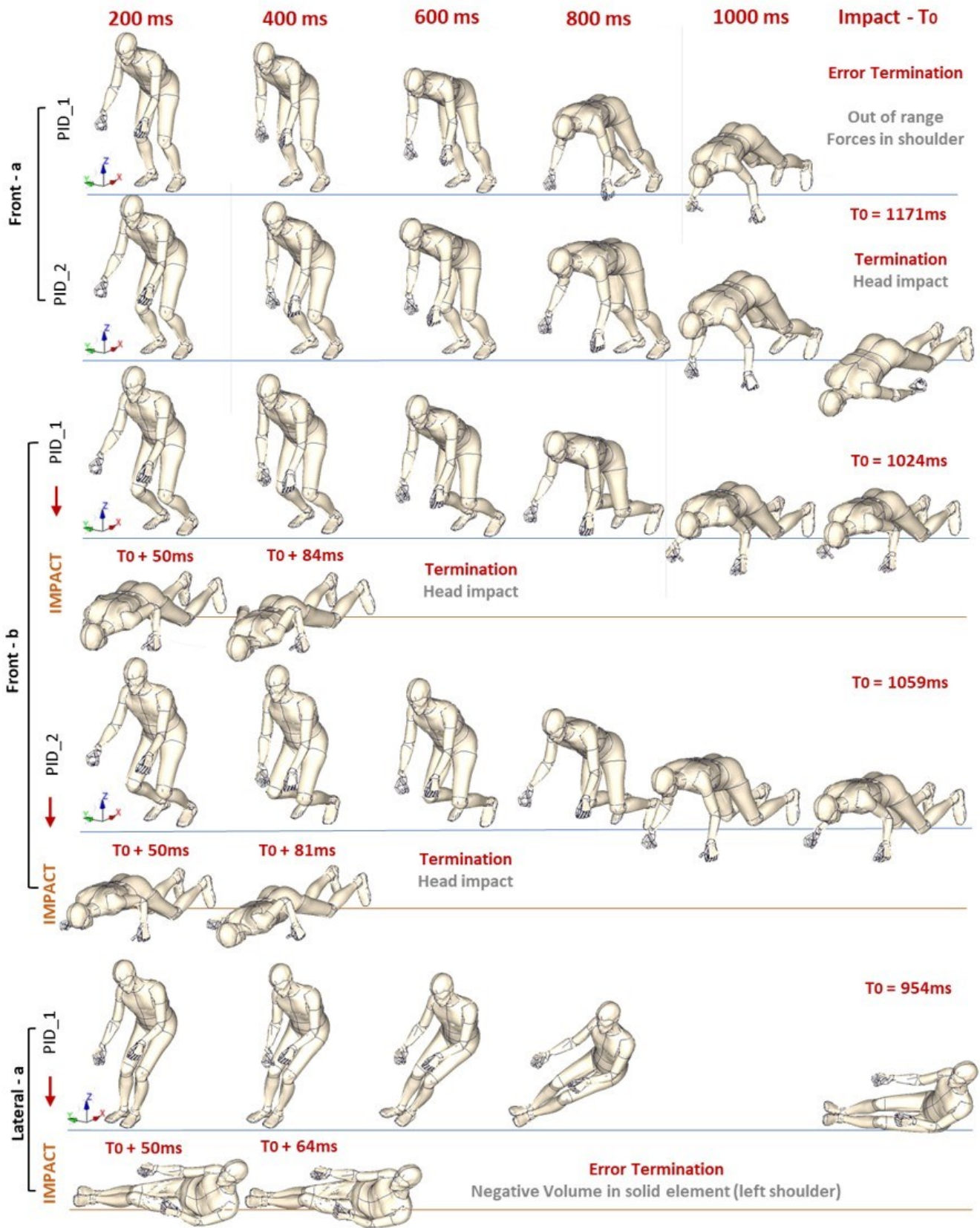
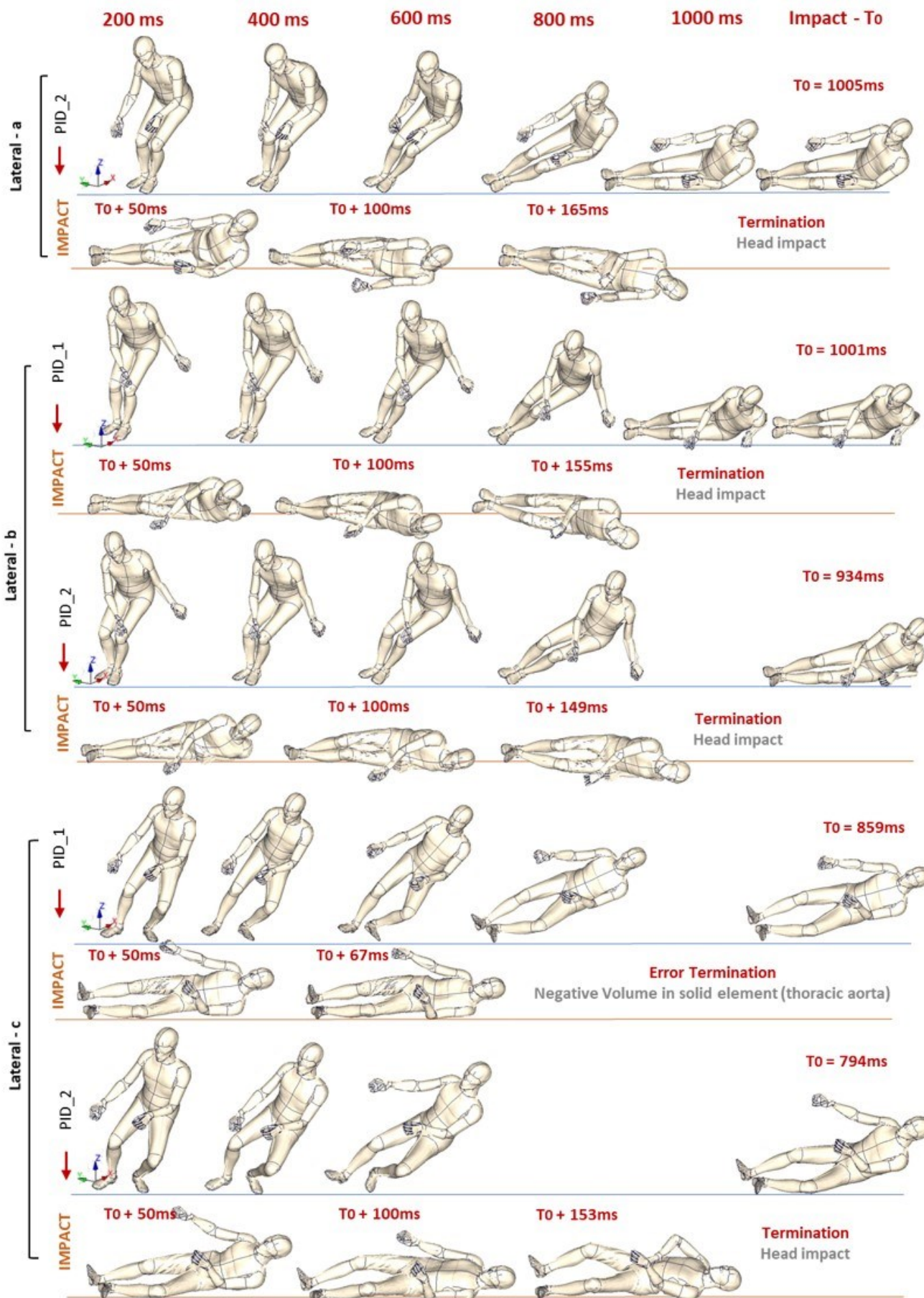
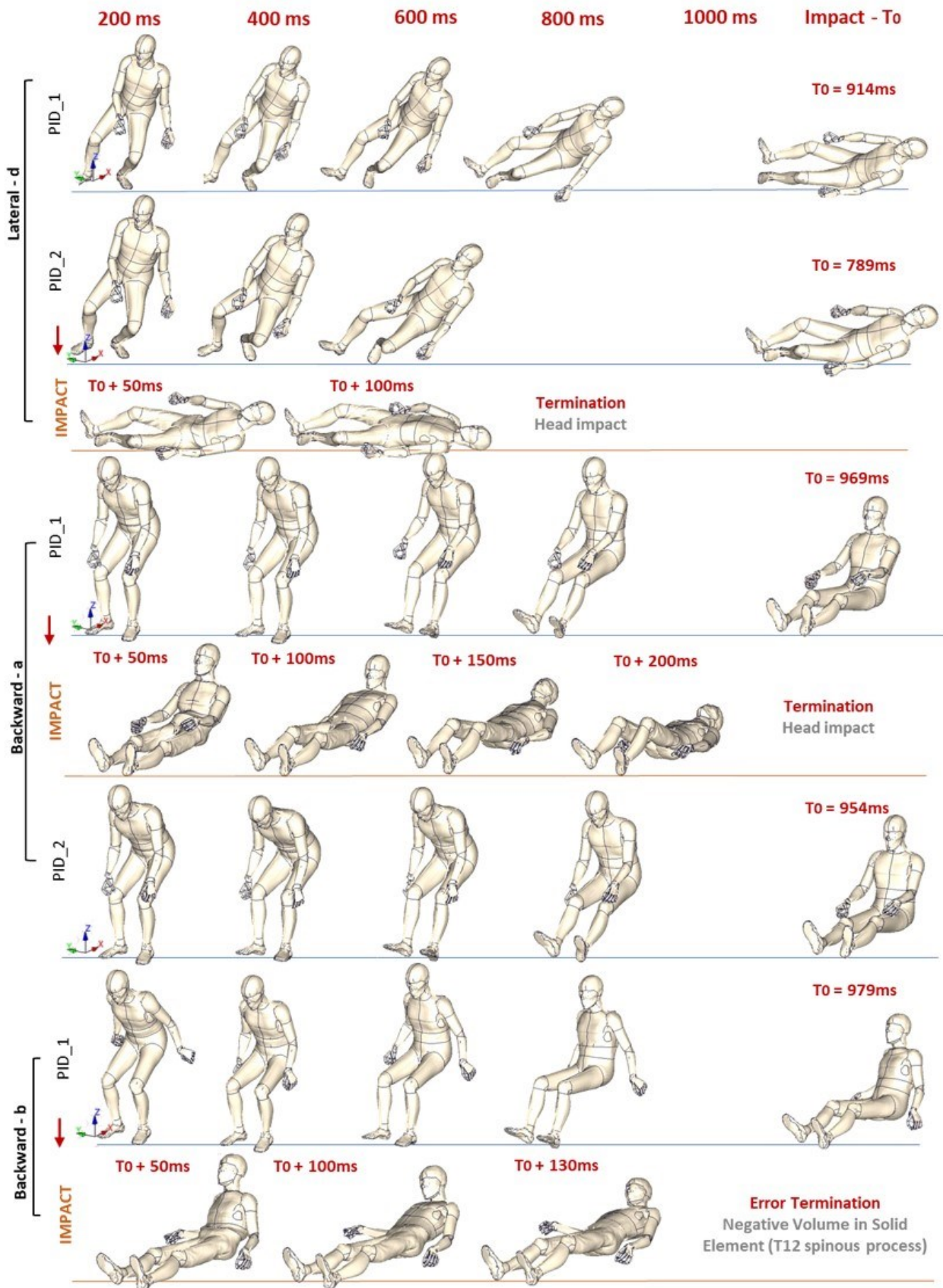


Fig. D1. Kinematics results of the impact verification simulations.

D2) Fall configurations







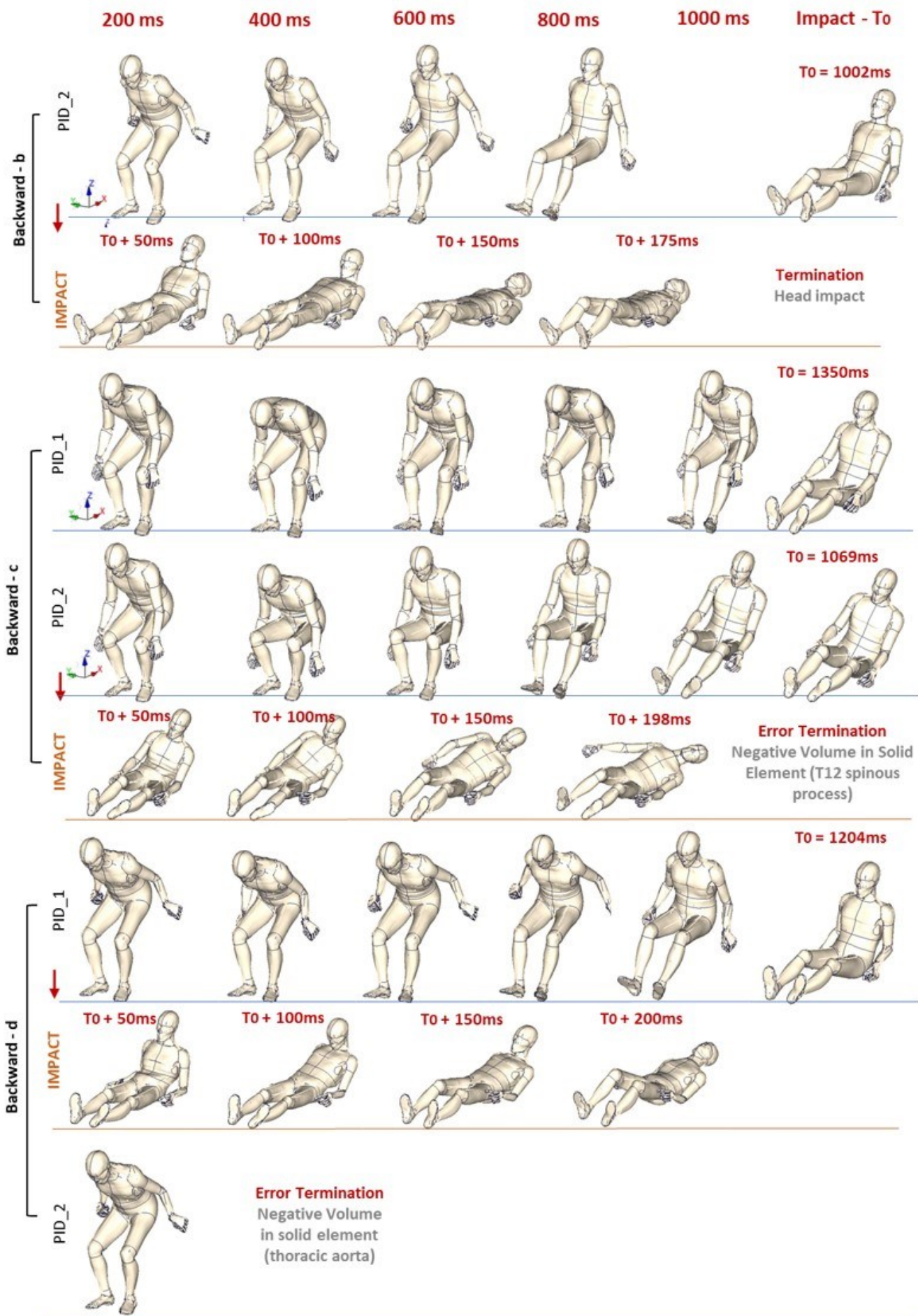


Fig. D2. Fall and impact kinematics

D3) Stumbling boundary conditions, kinematics and results

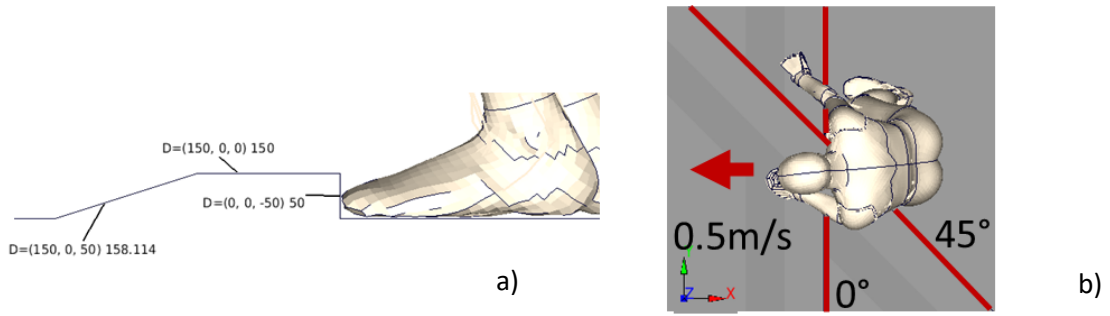


Fig. D3. Stumbling boundary conditions: a) The obstacle and its size (in mm), b) Initial velocity and the obstacle orientation variants (0°, 45°)

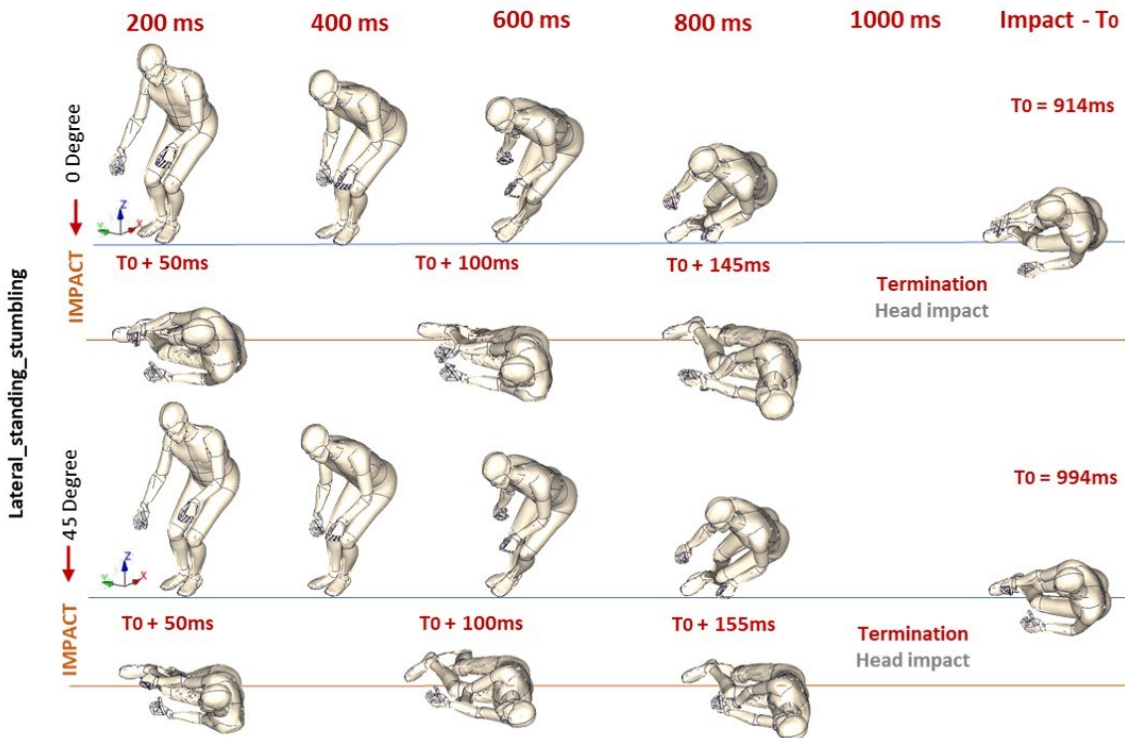


Fig. D4. Stumbling fall and impact kinematics

TABLE D3

STUMBLING: IMPACT RESULTS AND REFERENCE (LATERAL-A) COMPARISON

	Reference	0 - Stumble	45-Stumble
Horizontal Pelvic Velocities at t0 (m/s)	1.56	1.73	1.70
Vertical Pelvic Velocities at t0 (m/s)	2.70	2.79	2.89
Femur neck angles (°)	80.20	81.70	75.81
Sagittal pelvic angles (°)	31.60	19.85	16.99
Anterior pelvic angles (°)	71.95	85.11	87.42
Sagittal torso angles (°)	36.71	27.08	25.81
Posterior torso angles (°)	85.22	77.57	80.33
Maximum left femur neck Force (kN)	4.13	6.15	4.94
Maximum left femur neck moment (Nm)	85.07	116.72	104.41
Maximum pelvis acceleration (g)	55.10	88.59	76.14
Right femur neck force (kN)	1.17	1.15	0.92
L5 force (kN)	0.80	0.65	0.63
Maximum head velocity (m/s)	10.70	7.736	7.385
Head Injury Criteria (36ms)	2859.7	539.0	1420.6

Appendix E) Variants, Data Inclusion and Model Properties

		Front		Lateral				Backward			
		a) Protective arms	b) Protective arms + flexed knee	a) None	b) Protective arm	c) Flexed knee	d) Protective arm + flexed knee	a) None	b) Protective arm	c) Active Squating	d) Protective arm + Active Squating
Muscle Controller	PID1	Excluded		Impact S. -> Muscle A.	Impact S. -> Muscle A.	Impact S.		Impact S.	Impact S.		Act. Head impact
	PID2	Excluded		Impact S. -> Muscle A.	Impact S. -> Muscle A.	Impact S.	Impact S.		Impact S.	Impact S.	Error Termination
		Stumble 0°		Impact S. -> Muscle A.				Fall Kinematic Evaluation	Excluded for consistency	Excluded due to unrealistic behaviour	Impact S.: Impact simulations based on the fall kinematics
		Stumble 45°		Impact S. -> Muscle A.				Muscle A.: Impact simulations with Co-Contraction patterns		Act. Head Impact: Protective Flexion Simulations	

Musculoskeletal model testing	Low energy impact verifications	Fall Simulations	Impact Simulations	Muscle Activations (Co-Contraction)	Act. Head Impact
Original THUMS V502	Restarted from fall simulation (only for standing height)	Original THUMS V502	Restarted from fall simulation	Restarted from fall simulation	Restarted from fall simulation
Rigid bones	Deformable bones	Rigid bones	Deformable bones	Deformable bones	Deformable bones
Target joint angle offsets	Modified TST and material model (14 and 18mm)	Target joint angle offsets	Modified TST and material model (18mm)	Modified TST and material model (18mm)	Modified TST and material model (18mm)
PID controller	Passive muscle state in whole body	PID controller	Passive muscle state in whole body	Pre-defiend muscle activations on left hip muscles	PID Controller
				Remaining muscle are in passive state	Target joint angle offsets for protective flexion

Fig. E1. Variants Overview and model properties

Above stated, unrealistic behaviour refers to fall kinematics which results in an initial head impact prior to knee or hip contact. To the best of our knowledge, there is no observation to support such fall kinematics; therefore, it is considered unrealistic and excluded from the result evaluations.